

UC Berkeley

UC Berkeley Electronic Theses and Dissertations

Title

Molecular basis for multimerization in the activation of the epidermal growth factor receptor

Permalink

<https://escholarship.org/uc/item/80q6j5fj>

Author

Huang, Yongjian

Publication Date

2016

Peer reviewed|Thesis/dissertation

Molecular basis for multimerization in the activation of the epidermal growth factor receptor

By

Yongjian Huang

A dissertation submitted in partial satisfaction of the requirements for the degree of

Doctor of Philosophy

in

Biophysics

in the Graduate Division of the

University of California, Berkeley

Committee in Charge:

Professor John Kuriyan, Chair

Professor Jay T. Groves

Professor Ehud Y. Isacoff

Professor Michael Rape

Fall 2016

Abstract

Molecular basis for multimerization in the activation of the epidermal growth factor receptor

**by
Yongjian Huang**

Doctor of Philosophy in Biophysics

University of California, Berkeley

Professor John Kuriyan, Chair

The epidermal growth factor receptor (EGFR), and its relatives HER2, HER3 and HER4, are receptor tyrosine kinases that couple the binding of extracellular ligands to the initiation of intracellular signaling pathways that control cell growth and proliferation. Aberrant signaling from EGFR family members underlies the onset of many human cancers. The canonical view of EGFR activation is that the receptor is activated by dimerization. It is known, however, that EGFR activation also generates higher-order multimers, whose structural details and functional consequences are poorly understood. Due to the incomplete understanding of the significance of multimerization for EGFR activity, the monomer/dimer model has remained the paradigm for EGFR activation mechanism. In collaboration with Shashank Bharill, a postdoc in Ehud Isacoff's group, we now have characterized ligand-induced dimerization and multimerization of human EGFR using single-molecule based analysis, specifically, stepwise fluorescence photobleaching using EGFR transfected into *Xenopus* oocytes. This single-molecule technique was first developed in Isacoff lab back in 2007, for counting subunits of membrane proteins in live-cell by observing photobleaching steps of GFP that is fused to a protein of interest. Without disrupting their membrane environment, we have now been able to determine the stoichiometry of EGFR complexes before and after activation. Using mutations identified in this study that are specifically important for multimerization of EGFR, I uncovered a functional role for multimerization in EGFR activation. These mutations reduce EGFR autophosphorylation in mammalian cells, particularly for sites in the C-terminal tail that are proximal to the kinase domain, and they also attenuate phosphorylation of phosphatidylinositol 3-kinase, which binds to a proximal site on the EGFR C-terminal tail. In collaboration with Deepti Karandur, a postdoc in Kuriyan lab, we propose a structural model for EGFR multimerization that is consistent with our experimental observations, which might be applicable to other human EGFR family members as well. During the investigation of EGFR stoichiometry in the presence of EGF using *Xenopus* oocytes, we made an unexpected discovery. Upon binding to EGF, EGFR shows linear back-and-forth motion on the oocyte surface, which is dependent on EGFR kinase activity and the actin cytoskeleton. To fully uncover the mechanism behind the observed linear motion of EGFR, more extensive studies are needed.

Table of contents

Acknowledgements

Chapter 1 Introduction

- 1.1 The canonical model for the activation of EGFR
- 1.2 Studies on EGFR stoichiometry

Chapter 2 Analysis of the stoichiometry of human EGFR expressed in *Xenopus* oocytes in the absence of EGF

- 2.1 Human EGFR is expressed and analyzed on *Xenopus* oocytes surface
- 2.2 EGFR is predominantly monomeric in the absence of ligand
- 2.3 Probing the formation of ligand-independent EGFR dimers

Chapter 3 Observation of linear back-and-forth motion of EGFR expressed in *Xenopus* oocytes in the presence of EGF

- 3.1 EGF cannot diffuse efficiently between the oocyte and the coverglass
- 3.2 Addition of EGF induces linear motion of EGFR expressed in *Xenopus* oocytes
- 3.3 Surface features of the *Xenopus* oocytes plasma membrane
- 3.4 EGFR activity and actin cytoskeleton are required for linear motion of EGFR

Chapter 4 Analysis of the stoichiometry of human EGFR expressed in *Xenopus* oocytes in the presence of EGF

- 4.1 FLAG-tag helps in stabilizing the EGFR molecules expressed in *Xenopus* oocytes in the presence of EGF
- 4.2 Addition of EGF to EGFR generates dimers and higher-order multimers
- 4.3 Analysis of the role of the canonical dimer interface in EGFR multimerization
- 4.4 Identification of residues in Domain IV that are necessary for EGFR multimerization

Chapter 5 Functional role of multimerization in EGFR activation

- 5.1 Effects of Domain IV mutations on EGFR tail phosphorylation
- 5.2 Effects of Domain IV mutations on two effector proteins
- 5.3 Proximal and distal sites in EGFR tail are phosphorylated differently within a EGFR dimer
- 5.4 Lateral phosphorylation is inefficient between EGFR dimers
- 5.5 A model for multimerization in the activation of EGFR

Concluding Remarks

Materials and Methods

- Single-molecule imaging in live *Xenopus* oocytes
- Analysis of phosphorylation by flow cytometry
- Analysis of EGFR surface expression by fluorescence microscopy
- Docking of EGFR by ClusPro
- Molecular dynamics simulation of EGFR Tetramer

References

Acknowledgements

First and foremost, I must admit that I made numerous mistakes throughout my graduate school but fortunately, choosing my mentor/advisor isn't one of them. My Ph.D thesis project has steadily evolved over the years, so does our understanding and interest in the working mechanism of EGFR. My mentor John Kuriyan has always been supportive and insightful along the way. His genuine scientific curiosity and instinct, along with his obsessive pursuit of clarities and fundamentals in understanding the molecular mechanism of biological systems, never stop inspiring and challenging me to go deeper and further. Meanwhile, I truly appreciate the free and collaborative working environment offered by Kuriyan lab.

The major portion of the work that I present in this dissertation, is resulted from a very fruitful collaboration with Ehud Isacoff's group here at Berkeley. I want to thank Ehud Isacoff for his inspirational and critical insights into this project at all stages. I also want to thank Shashank Bharill, who is my collaborator on this project from Ehud Isacoff's group. His expertise in single-molecule fluorescence microscopy and his persistent interest in studying membrane receptor initiated signal transduction, make our collaboration possible and pleasant.

I also want to thank Adam Smith and his group at University of Akron, for their helpful discussion and key contribution in this project. They used pulsed-interleaved excitation fluorescence cross-correlation spectroscopy (PIE-FCCS) to study human EGFR transfected into mammalian COS-7 cells.

Kuriyan lab member Deepti Karandur and Sean Peterson both made significant contributions to this project. Deepti designed and conducted the docking of EGFR extracellular domains. She also built the model for the whole EGFR tetramer and ran the molecular dynamics simulation of it. Sean experimentally confirmed that our reported EGFR multimer disruption mutations, did not cause mislocalization of receptors. Both Deepti's and Sean's results are described in Chapter 5.

As an international student here in the United States, the odds of getting a pre-doctoral fellowship is rather slim. Fortunately, the Howard Hughes Medical Institute (HHMI) launched an International Student Research Fellowships Program back in 2011. Between 2012-2015, I was financially supported by this program. For 2015-2016, I was funded by the University of California Cancer Research Coordinating Committee (CRCC) Predoctoral Fellowship.

Dedication

During the period while I am writing this dissertation and trying to present here the major part of my graduate work, my wife Xiaozhu gave the birth to our second daughter, Nicole. Our elder daughter Emma is very excited about her younger sister too. It is often too easy for me to ignore that the past six years have been a very eventful stretch in my life. And I am truly thankful that these beautiful ladies have always been there with me through the highs and lows.

I also want to thank my parents for their endless support.

Chapter 1 Introduction

1.1 The canonical model for the activation of EGFR

The epidermal growth factor receptor (EGFR) is a receptor tyrosine kinase that couples the binding of extracellular ligands, such as EGF and transforming growth factor- α (TGF- α), to the initiation of intracellular signaling pathways that control cell growth and proliferation (Kovacs et al., 2015a; Leahy, 2004; Lemmon et al., 2014), such as the mitogen-activated protein kinase (MAPK) pathway and the phosphatidylinositol 3-kinase (PI3K)/Akt pathway.

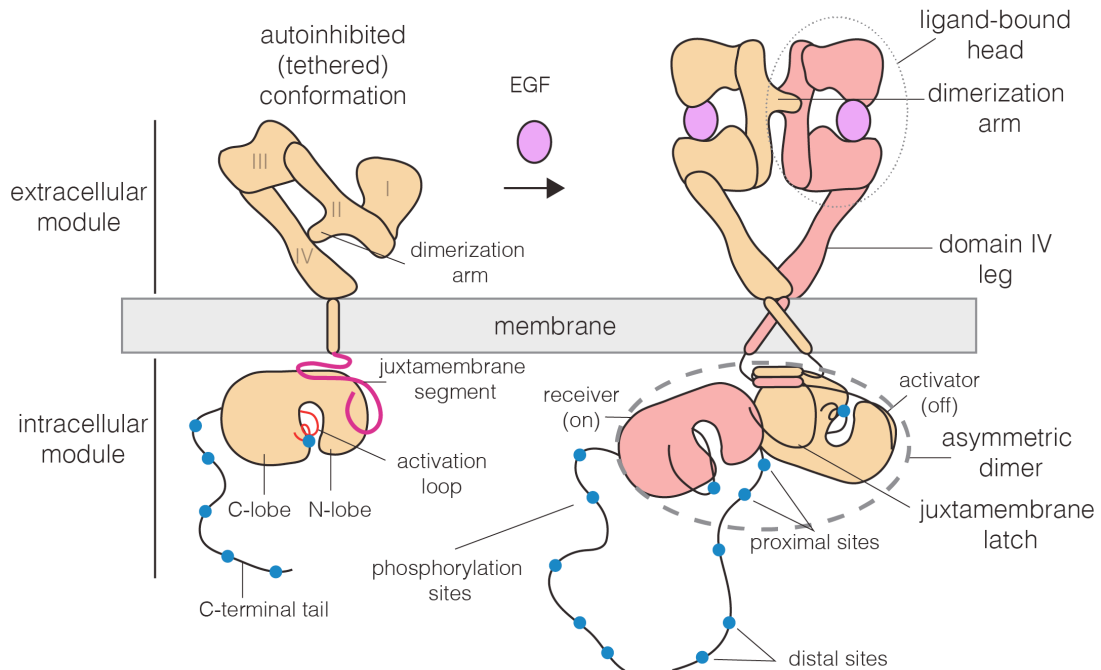
Human EGFR is one of four closely-related receptors that form homodimeric or heterodimeric combinations (Yarden and Sliwkowski, 2001). EGFR and one other member of the family (human epidermal growth factor receptor 4, HER4, also known as ErbB4) can bind to specific ligands, and respond by activating their intracellular kinase domains. The two other members of the family, HER2 and HER3, are potent signaling receptors in combination, with HER3 switching on the kinase activity of HER2 in response to ligands binding (Citri et al., 2003; Sliwkowski et al., 1994). Aberrant signaling from EGFR family members underlies the onset of many cancers, and there is intense interest in understanding how these receptors are regulated (Lynch et al., 2004; Paez et al., 2004; Pao et al., 2004; Slamon et al., 2001).

The canonical view of EGFR activation considers the monomeric receptor to convert to a dimeric form upon the addition of EGF (Lemmon et al., 1997; Schlessinger, 2002; Yarden and Schlessinger, 1987a, 1987b) (Figure 1A). Ligand-induced receptor dimerization activates the intracellular kinase domains of the receptor, resulting in autophosphorylation of a ~230 residue C-terminal tail and the initiation of downstream signaling (Margolis et al., 1989). The extracellular module of EGFR consists of four domains, denoted Domains I, II, III and IV (Figure 1A and 1B). Domains I and III form the ligand-binding site of the receptor (Garrett et al., 2002; Lu et al., 2010; Ogiso et al., 2002). Domain II, which bridges the ligand-binding domains, contains a “dimerization arm” that interacts with the corresponding element in the other subunit in a dimer (Dawson et al., 2005). Domains I, II and III form a compact unit that I refer to as the “head” of the extracellular module, of which Domain IV forms an elongated “leg”. In the absence of ligand, the extracellular module adopts a tethered and autoinhibited conformation, in which the dimerization arm is buried between the head and the leg (Ferguson et al., 2003), forming an intramolecular interaction between Domain II and IV. Ligand binding converts the receptor to a straightened conformation, releasing the dimerization arm, which then interacts to form a back-to-back dimer in which ligands do not participate directly in the inter-subunit interfaces.

On the intracellular side, activation of the receptor involves the formation of an asymmetric dimer of kinase domains, in which one kinase serves as a cyclin-like allosteric activator of the other (Jura et al., 2009a, 2011; Red Brewer et al., 2009; Zhang et al., 2006). This allosteric interaction involves the C-lobe of one kinase (the “activator”) forming a tight interface with the N-lobe of another (the “receiver”), which stabilizes the receiver in an active conformation (Figure 1A). The transmembrane helices, which connect the extracellular module to the intracellular module, also dimerize (Mendrola et al., 2002; Mineev et al., 2010), and this dimer is coupled to the formation of the asymmetric dimer of kinase domains (Arkhipov et al., 2013a; Endres et al., 2013; Jura et al., 2009a). This model for EGFR dimerization explains how a

variety of ligands can activate the receptor, how heterodimeric combinations of the four EGFR family members can form, and how the catalytically impaired member of this family, HER3, can activate HER2 (Endres et al., 2014; Jura et al., 2009b; Kovacs et al., 2015a; Shi et al., 2010). Upon activation, EGFR kinase domains autophosphorylate multiple tyrosine residues on the C-terminal tail of the receptor. These phosphorylated tyrosine residues will serve as docking sites for downstream signaling adaptor proteins and effector proteins, which can bind to phosphorylated tyrosine sites through SH2 (Src homology region 2) and PTB (phosphotyrosine-binding) domains.

A



B

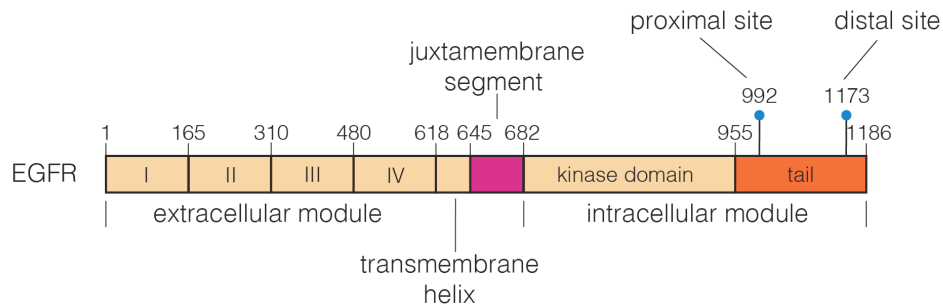


Figure 1 Schematic diagrams of EGFR structure.

(A) The canonical model for the monomer to dimer transition in EGFR that is triggered by ligand binding (Kovacs et al., 2015a; Lemmon et al., 2014). (B) Domain boundaries in human EGFR. The residue numbers do not include the 24 residue signal sequence. (Adapted from eLife 2016;5:e14107)

1.2 Studies on EGFR stoichiometry

Like many other membrane proteins, the stoichiometry of EGFR complexes is highly regulated and is critical to its functional states. It has been experimentally demonstrated that EGFR is primarily monomeric prior to ligand binding (Endres et al., 2013; Nagy et al., 2010). Although pre-formed unliganded EGFR dimers were also reported (Clayton et al., 2007; Kozier et al., 2011; Nagy et al., 2010), little is known about the structural and functional characteristics of pre-formed EGFR dimers.

On the other hand, the oligomeric states of EGFR upon activation is still unclear. Membrane protein stoichiometry was traditionally indirectly derived from bulk biochemical and ensemble-averaged functional analyses. Early studies on the stoichiometry of EGFR was done by running EGFR samples purified from cells on native gels, and the EGFR association states were estimated based on the sample migration pattern seen in the native gels. Similarly, crosslinked EGFR samples were analyzed by denaturing gels (Yarden and Schlessinger, 1987a, 1987b). The binding characteristics of EGF to EGFR was also used to infer the stoichiometry of EGFR complexes (Yarden and Schlessinger, 1987b). In their seminal analysis of the activation of EGFR by EGF, Yarden and Schlessinger showed that the addition of EGF to EGFR results in the formation of dimers or higher-order multimers in cells (Yarden and Schlessinger, 1987a, 1987b). Later, various techniques based on bulk fluorescence measurements were utilized to extract quantitative information regarding the EGFR oligomerization states (Clayton et al., 2005, 2008; Kozier et al., 2013). More recently, single-molecule fluorescence microscopy was used to directly visualize the EGFR clustering (Chung et al., 2010).

Although traditional discussion of the activation of EGFR has focused on a monomer to dimer transition, Clayton, Burgess and colleagues concluded that EGFR forms tetramers upon activation, and that the tetramers are essential for downstream signaling (Clayton et al., 2005, 2008; Kozier et al., 2013). In these studies, the authors used image-correlation spectroscopy to extract the relative association state of activated versus unactivated EGFR. They found that, on average, there were at least four times as many receptors in the activated clusters than unactivated clusters. These authors also used lifetime-detected Förster resonance energy transfer (FRET), to probe Grb2 binding to activated EGFR clusters and found that Grb2 were associated with EGFR tetramers.

Another single-molecule tracking study of EGFR in live cells also showed that EGFR forms large clusters after activation (Chung et al., 2010). In this study, the authors tagged EGFR molecules with a quantum dot linked to an anti-EGFR antibody Fab fragment, and optically tracked the diffusion of EGFR molecules. They found that unliganded EGFR diffuses in two different states, a fast diffusing “monomer state” and a slow diffusing “dimer state”. In the presence of EGF, EGFR exhibits an EGF-induced very slow diffusion state that is much slower than the “dimer state”. This indicates the formation of EGFR clusters that are larger than dimers.

Thus, higher-order multimerization and clustering are important correlates of EGFR activation, but the structural details and functional consequences of these larger assemblies are not clear. While there is not much debate about their existence, higher-order EGFR assemblies remain elusive to direct visualization and structural characterization. Without knowing the structural details of these assemblies, it is even more challenging to investigate their functional role in EGFR signaling, because mutations that specifically inhibit EGFR higher-order clustering have not been identified.

The direct determination of EGFR complex stoichiometry faces some major challenges. Firstly, the membrane environment is highly involved in regulating EGFR function and therefore, the stoichiometry of EGFR complexes should be assessed on cell membrane. For example, the complex EGF binding characteristics seen on cell membrane, featuring concave-up Scatchard plots that indicates either negative cooperativity or different classes of EGF-binding sites with distinct affinities, is lost when the extracellular domain of EGFR is studied in isolation (Alvarado et al., 2010; Bessman et al., 2014; Macdonald and Pike, 2008; Ozcan et al., 2006; Pike, 2012). On the intracellular side, the EGFR kinase domain was reported to be regulated by its potential interaction with membranes (Arkhipov et al., 2013a; Endres et al., 2013). Secondly, the traditional cell fixation procedures should be avoided, unless their effects on the protein of interest and plasma membrane have been sufficiently characterized.

Preferably, the stoichiometry of EGFR complexes should be determined on live-cell membranes without fixation. Fixation could introduce artifacts because the dynamics of the local membranes, which could play important role in regulating EGFR function, is basically frozen after the fixation. That includes the changes of membrane fluidity, lipid composition, charge distribution, curvatures, and so on. Additionally, typical fixatives are also known to cause various imaging artifacts by inducing nonspecific protein aggregation and membrane deformation. The ratio of fluorescence labeling molecule to EGFR molecule is critical in determining the stoichiometry and ideally, this ratio should be 1:1. Due to the high surface density of EGFR expressed on mammalian cell membranes, most single-molecule based studies are forced to label only a tiny fraction of EGFR molecules on the cell surface, by incubating the cells with very low concentration of fluorescently-labeled EGF or anti-EGFR antibody. Under this labeling scheme, only a very small portion of EGFR molecules are selectively visualized at a time, while the majority of molecules remains dark and invisible. Information extracted based on the observation of those selected a few can only provide an indirect and rough estimation for the association states of the whole population.

In collaboration with Shashank Bharill in Ehud Isacoff's group, I analyzed the stoichiometry of EGFR complexes before and after activation, using stepwise photobleaching of fluorescently-tagged proteins expressed in *Xenopus* oocytes (Chen et al., 2015; Ulbrich and Isacoff, 2007). This single-molecule technique was first developed in the Isacoff lab about ten years ago, and it provides a powerful tool for quickly determining subunit stoichiometry of membrane proteins in live-cells by directly counting discrete photobleaching steps of GFP tags that are fused to the protein of interest. The GFP fusion of the protein of interest was expressed in *Xenopus leavis* oocytes. The use of the genetically encoded GFP ensures that there is exactly one chromophore attached to each targeted protein. This effectively fixes nonspecific labeling issues suffered by the use of organic dyes or quantum dots. The guaranteed 1:1 ratio of GFP and target protein also eliminates any over- or sub-sampling of the target protein, except for variation in the fraction of GFP that is properly matured. Thus the number of GFP photobleaching steps within one protein complex is correlated with the number of GFP-tagged target protein in the complex, subject to a correction for GFP maturation rate.

Total internal reflection fluorescence (TIRF) microscopy was used to restrict illumination to the interface between the coverslip and the cell, which limits the measurement to the fraction of target proteins that are on the cell membrane. Another advantage of using TIRF is to reduce the autofluorescence from the cell cytoplasm, which increases the signal to noise ratio of data. The use of *Xenopus leavis* oocytes for expression further reduces the background fluorescence, because the dark pole of *Xenopus leavis* oocytes shows extremely low autofluorescence. Another

critical advantage offered by *Xenopus leavis* oocytes is that the expression level of target membrane proteins could be readily controlled, in order for them to be evenly and sparsely spaced for single molecule study. The combination of these advantages enabled us to make a definitive advance in understanding EGFR stoichiometry.

We find that EGFR exists as a monomer prior to ligand binding. Addition of EGF results predominantly in higher-order multimers, rather than just dimers. We have identified, through modeling and mutagenesis, a region within Domain IV of the extracellular module that is important for multimerization of the receptor, but is not required for dimerization. These data suggest that EGFR multimers are comprised of EGFR dimers that self-associate through Domain IV to form higher-order assemblies.

In collaboration with Adam Smith's group at University of Akron, we also used pulsed-interleaved excitation fluorescence cross-correlation spectroscopy (PIE-FCCS) (Müller et al., 2005; Smith, 2015) to study human EGFR transfected into mammalian COS-7 cells. I show that EGF addition to EGFR in COS-7 cells results in the formation of multimers, rather than just dimers. Importantly, introduction of a Domain IV mutation that blocks multimerization of EGFR in the *Xenopus* oocyte assay prevents the formation of multimers in mammalian cells, with the response to EGF of the mutant EGFR being limited to dimer formation. Since the main body of work regarding the PIE-FCCS was done by Adam Smith's group at University of Akron, I do not include a discussion of these data in this dissertation.

I tested the functional importance of multimer formation for EGFR activity in a human cell line (HEK-293). The mutations in Domain IV that reduce multimerization also reduced phosphorylation of Tyr 992, a site in the C-terminal tail that is proximal to the kinase domain, and Tyr 1173, a distal site. These mutations attenuate the phosphorylation of phosphatidylinositol 3-kinase (PI3K), which is reported to bind to Tyr 992 (Jones et al., 2006). In contrast, the phosphorylation of extracellular signal-regulated kinase (ERK), which is activated through phosphorylation of distal tyrosine sites on the EGFR C-terminal tail (Batzer et al., 1994), is not affected by these mutations. My data suggest that this differential effect on proximal phosphorylation may arise from the structure of the asymmetric dimer of kinase domains, in which the proximal sites on the activator kinase cannot reach the active site of the receiver kinase, and would therefore be poorly phosphorylated in isolated dimers. I speculate that multimerization results in the formation of chains of kinase domains, in which the majority of kinase domains would be stabilized in the active conformation, allowing stronger phosphorylation in general, and more complete phosphorylation of proximal sites *in cis*.

In collaboration with Deepti Karandur, a postdoc in our lab, we have constructed a model for a ligand-bound EGFR tetramer, using several criteria that emerged from my experiments. This model generates a spacing between dimers of the extracellular domain that is consistent with linkage to a head-to-tail chain of kinase domains, which serve as receivers and activators for each other. The tetramer constructed in this way is open-ended, and can potentially engage additional dimers to extend the chain to form larger scale multimers and clusters.

Chapter 2 Analysis of the stoichiometry of human EGFR expressed in *Xenopus* oocytes in the absence of EGF

Introduction

The work on determining EGFR stoichiometry that I present in Chapter 2, 3 and 4 resulted from a close collaboration with Shamsankh Bharill, a postdoc in Ehud Isacoff's group. In this Chapter, I describe the *Xenopus* oocyte assay system that we developed and show that EGFR is predominantly monomeric in the absence of EGF. We also looked into the nature of a small population of EGFR molecules that are dimerizing in the absence of EGF.

2.1 Human EGFR is expressed and analyzed on *Xenopus* oocytes surface

We measured EGFR stoichiometry by transient transfection in *Xenopus* oocytes, which provides a convenient experimental system for controlled and reliable protein expression at very low levels (Ulbrich and Isacoff, 2007). It has been shown previously that human EGFR reconstituted into *Xenopus* oocytes is fully functional, and that the oocytes lack endogenous EGFR expression (Opresko and Wiley, 1990). For the *Xenopus* assay we made EGFR constructs that are fused at the C-terminus to EGFP, a monomeric variant of GFP that has enhanced fluorescence (Yang et al., 1996). We expressed EGFR-EGFP (I shall simply refer to this construct as EGFR, and to EGFP as GFP) in *Xenopus* oocytes, and used TIRF microscopy to image the animal pole of the oocyte (Figure 2A). The animal pole of the oocyte contains dark pigments, which results in extremely low auto-fluorescence background during TIRF imaging.

In a typical experiment, we observe well-separated spots of GFP fluorescence intensity corresponding to EGFR. The spots are stable in position, allowing their photobleaching properties to be studied readily. The surface density of the receptor is estimated to be ~ 1 to ~ 5 molecules per μm^2 (Figure 2). The effective local density of EGFR may be higher, because the membrane surface of the oocytes forms microvilli, within which the receptors are located (Heinzmann and Höfler, 1994; Sonnleitner et al., 2002). Nevertheless, the expression level of EGFR in these cells is very low when compared to that seen in typical mammalian-cell based experimental systems. For comparison, the surface densities of EGFR in the cancer cell lines A431, HeLa and A549 are ~ 600 , ~ 300 and ~ 100 molecules per μm^2 , respectively (Zhang et al., 2015).

To monitor photobleaching, a $13 \mu\text{m} \times 13 \mu\text{m}$ field of view was illuminated in the TIRF mode by a laser and movies of 500-800 frames were recorded at a frame rate of 20 Hz. Frames from these movies were analyzed to measure the time-dependent changes in the fluorescence intensities of individual spots, as shown in Figure 2. Analysis was restricted to spots that showed no overlap with nearby spots.

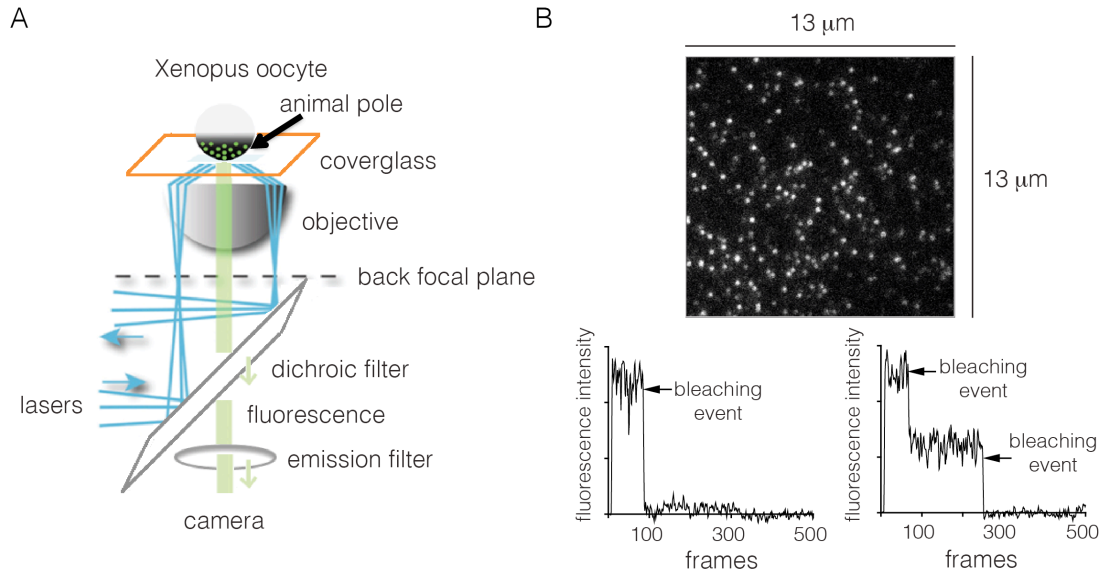


Figure 2 Monitoring the stoichiometry of human EGFR in Xenopus oocytes by photobleaching.

(A) Schematic diagram illustrating the analysis of transiently-transfected EGFR by TIRF microscopy. A single oocyte is placed on a glass coverslip for observation and evanescent wave excitation is elicited by total internal reflection of the laser beam. The bright spots represent fluorescence from the EGFP fused to the C-terminus of EGFR. (B) Representative photobleaching traces of individual spots for EGFR without EGF. Shown above is a single image from a movie of the field of view. The two graphs show examples of one-step (left) and two-step (right) photobleaching events. Frames collected at 20 Hz over 25 s. (Adapted from eLife 2016;5:e14107)

2.2 EGFR is predominantly monomeric in the absence of ligand

In the absence of ligand, most spots undergo photobleaching in a single step, although some are observed to decay in two steps (Figure 2B). We do not see any spots with more than two steps in the photobleaching traces. We analyzed over 900 individual spots from ~15 cells to generate a histogram of one-step and two-step photobleaching events, which shows that ~94% of the spots show a single step-wise reduction in fluorescence intensity to baseline levels (Figure 3A). We conclude that the receptor is predominantly a monomer in the absence of ligand, at the expression level of this experiment.

We estimated the fraction of two-step photobleaching events that would occur due to random colocalization of non-interacting proteins. To do this, we expressed Claudin-16, a transmembrane protein that is known to be monomeric (Gong et al., 2015), at a level comparable to that for EGFR in our experiments, and counted the number of one-step and two-step photobleaching events. For Claudin-16, ~3% of the spots show two-step photobleaching. We subtracted this baseline fraction of two-step bleaching events from all the data shown in Figure 3. With this correction, the fraction of two-step photobleaching events for EGFR is ~3% (Figure 3A). This is comparable to the level of ligand-independent preformed dimers reported in mammalian cells expressing EGFR at low levels (Nagy et al., 2010). Note that ~25% to ~35% of EGFP molecules are dark, due to incomplete maturation of the fluorophore, which results in fewer photobleaching steps than the number of subunits in a multimer (Ulbrich and Isacoff, 2007). Thus, two-step photobleaching may arise from dimers as well as a small population of higher-order multimers.

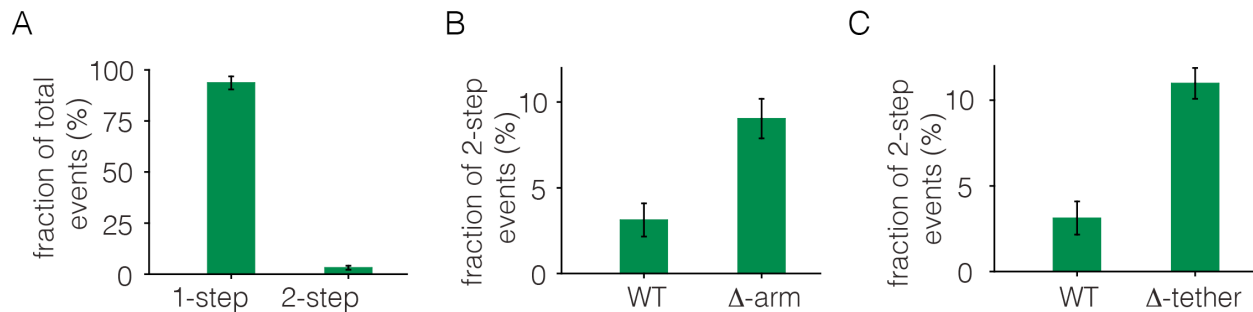


Figure 3 Analysis of photobleaching events for EGFR without EGF, in the Xenopus assay.

(A) Histogram of one-step and two-step photobleaching events for wild-type EGFR in the absence of EGF. This histogram represents the number of counted events. For subsequent analysis, the fraction of two-step events (3%) seen for a monomer control protein (Claudin-16) in the same experiment at a comparable density was subtracted from the fraction of two-step events seen for EGFR and EGFR variants. The fraction of two-step photobleaching events for wild-type EGFR (WT) is compared to that for mutants. (B) Δ -arm, deletion of the dimerization arm, residues 242 to 259. (C) Δ -tether, mutation in Domain IV that breaks the autoinhibitory interaction, (D563A, H566A and deletion of residues 575 to 585). (Adapted from eLife 2016;5:e14107)

2.3 Probing the formation of ligand-independent EGFR dimers

The nature of ligand-independent dimers of EGFR is of interest because overexpression of EGFR and other family members results in constitutive activation of the receptor. To probe the nature of the assembly that gives rise to the two-step photobleaching events, we first studied the role of the extracellular domain. We deleted the dimerization arm of the extracellular module, involving residues 242-259 (the mutant is denoted Δ -arm). This resulted in an increase in the fraction of two-step photobleaching events, from ~3% to ~9% (Figure 3B). The increase in apparent dimerization upon deletion of the dimerization arm is unexpected, given that that this element forms a major part of the extracellular dimer interface. A possible explanation is that the dimerization arm is also important for maintaining the tethered and autoinhibited conformation of the extracellular module, and deletion of the dimerization arm is expected to release autoinhibition, and thereby facilitate dimerization (Ferguson et al., 2003). To test this idea we introduced mutations on the other side of the tethered interaction, which is in Domain IV rather than in the dimerization arm of Domain II. I introduced two point mutations (D563A, H566A) and also deleted a loop (residues 575 to 585) in Domain IV. A similar mutation in EGFR has been shown to abolish the tethering interaction (Dawson et al., 2007). This mutation, which we refer to as Δ -tether, has the dimerization arm intact, and it also increases the fraction of two-step bleaching events (Figure 3C). These results are consistent with the accepted view, which is that the autoinhibited conformation of the extracellular domain provides a steric block to dimerization (Ferguson et al., 2003). Once this block is released, the extended shape of the extracellular module permits dimerization even if the dimerization arm is deleted.

We then studied the role of the kinase domain in ligand-independent dimerization. We introduced two kinds of mutations, based on alternative models for dimerization of the kinase domain. One mutation (V924R, in the C-lobe of the kinase domain) prevents the kinase from taking the activator position in an asymmetric dimer. We also introduced two mutations that are

expected to break a previously observed inactive dimer of kinase domains (the deletion of the AP-2 helix in the C-terminal tail (residues 969 to 978), denoted Δ tail-1, or deletion of the C-terminal tail in its entirety (residues 965 to 1186), denoted Δ tail-2) (Jura et al., 2009a; Kovacs et al., 2015b). The V924R mutation, introduced in the background of wild-type EGFR, resulted in a reduction of the fraction of two-step photobleaching events, from $\sim 3\%$ to $\sim 1.5\%$ (Figure 4A). The V924R mutation also reduced the fraction of two-step events for EGFR that was mutated in the autoinhibitory Domain II/IV intramolecular tethering interface (Figure 4D). The two deletions involving the C-terminal tail had no effect on the fraction of two-step events (Figure 4B). These results indicate that the ability of the kinase domains to form the asymmetric dimer of kinase domains underlies ligand-independent self-association of the receptor in our experiments.

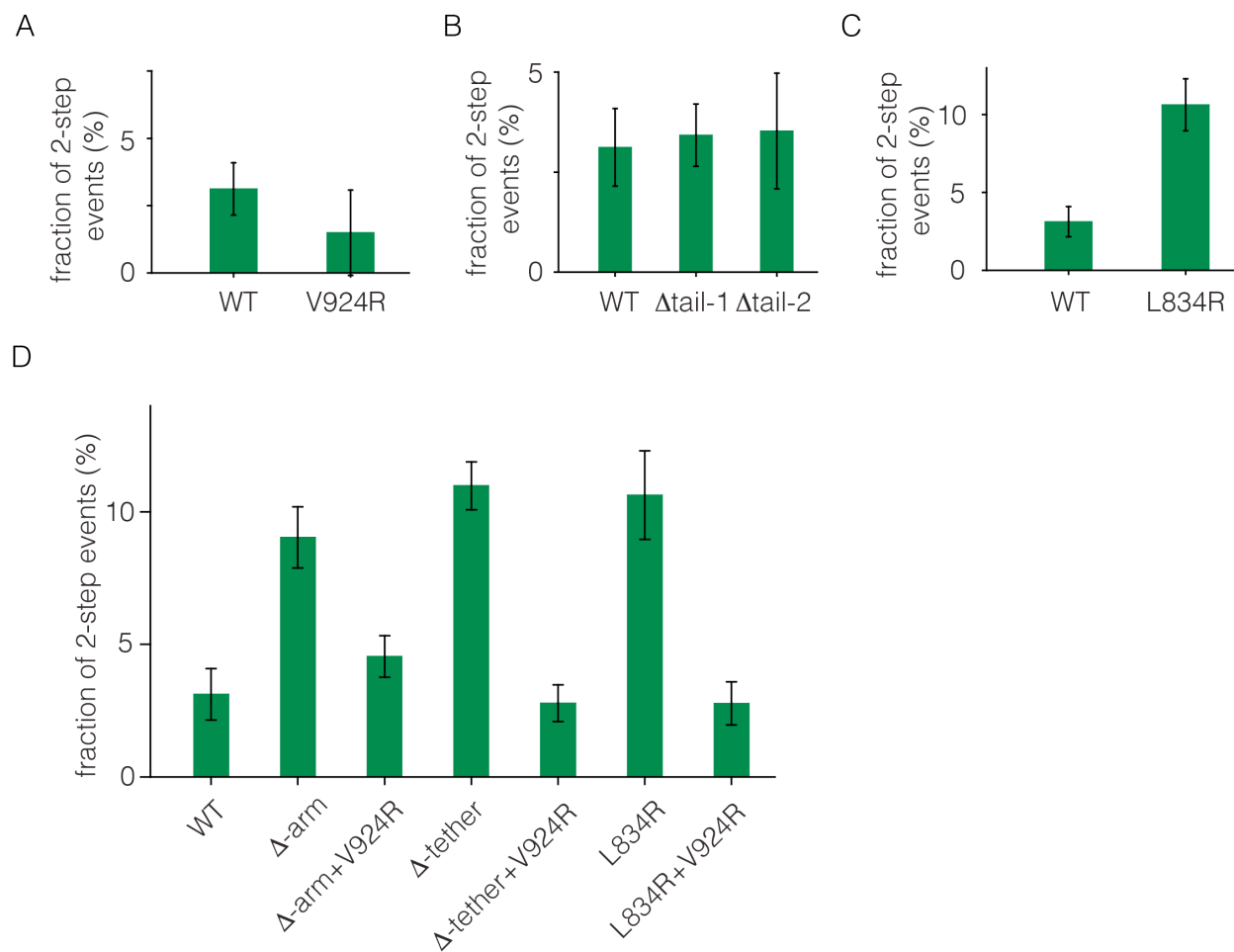


Figure 4 Effects of EGFR mutations on the EGF-independent two-step photobleaching events.

(A) V924R, mutation in the C-lobe of the kinase domain that prevents asymmetric dimer formation. (B) Δ -tail1, deletion of the AP-2 helix in the C-terminal tail (residues 969 to 978). Δ -tail2, deletion of the entire C-terminal tail (residues 965 to 1186). The Δ -tail1 and Δ -tail2 mutations were designed to disrupt a previously described dimer of inactive kinase domains (Kovacs et al., 2015b). (C) L834R, a mutation in the kinase domain that activates EGFR (Red Brewer et al., 2013). (D) Importance of the asymmetric dimer of EGFR kinase domains in generating two-step photobleaching events in the absence of EGF. The histogram shows the fraction of two-step photobleaching events for wild-type (WT) EGFR, compared to various mutants. Disruption of the dimerization arm (Δ -arm) or mutations in Domain IV (Δ -tether), or introduction of the activating L834R mutation in the kinase domain, increases the fraction

of two-step event, as also shown in Panels B to F. The introduction of the V924R mutation, which blocks asymmetric dimer formation, on top of these mutations reduces the extent of two-step events back to a level similar to that for the wild-type protein. (Adapted from eLife 2016;5:e14107)

We also studied the effect of an activating mutation in the kinase domain, L834R, which is commonly found in cancer patients harboring mutations in EGFR. This mutation stabilizes the active conformation of the kinase domain, and thereby favors the formation of the asymmetric kinase domain dimer (Red Brewer et al., 2013; Shan et al., 2012). The L834R mutation results in an increase in the fraction of two-step bleaching events (Figure 4C). This is consistent with a recent study showing that, L834R mutation drives ligand-independent activity through enhanced dimerization (Valley et al., 2015). Introduction of the V924R mutation in the background of the L834R mutation, the Δ -arm mutation or the Δ -tether mutation, results in a reduction in the fraction of apparent dimers (Figure 4D). These results further emphasize the importance of asymmetric dimer formation by the kinase domains in driving EGFR dimerization, even without the addition of EGF.

Summary

Using single-molecule based stepwise photobleaching assay, we show that EGFR is predominantly monomeric in the absence of EGF. This is consistent with the canonical model of EGFR activation, in which the ligand-free EGFR is monomeric. Additionally, we observed a small population of EGFR molecules that shows two-step photobleaching in our *Xenopus* oocyte assay. These two-step photobleaching events provide us a probe to monitor the nature of ligand-independent EGFR dimers, whose structure and function are difficult to study and poorly understood. Our results indicate that the autoinhibited conformation of extracellular domain prevents the receptor from dimerizing, while asymmetric dimer formation by the kinase domains is promoting the association between EGFR molecules in the absence of EGF.

Chapter 3 Observation of linear back-and-forth motion of EGFR expressed in Xenopus oocytes in the presence of EGF

Introduction

In this Chapter, I describe an unexpected discovery that we made during our investigation into EGFR stoichiometry in the presence of EGF. We observed a linear back-and-forth motion of EGFR on the Xenopus oocyte surface, that is triggered by the addition of EGF. We found the cellular basis for the linearity of this back-and-forth motion. Further studies reveal that EGFR kinase activity and the actin cytoskeleton are necessary for this phenomenon to happen.

3.1 EGF cannot diffuse efficiently between the oocyte and the coverglass

To study the stoichiometry of EGFR expressed in Xenopus oocytes in the presence of EGF, we added 15 nM EGF to the imaging chamber and immediately started to image the animal pole of the Xenopus oocytes. Surprisingly, we did not observe any noticeable changes in the fluorescence intensity of EGFR spots, which looked similar to what we saw in the absence of EGF. Then we used fluorophore-labeled EGF to trace where the ligand binds to the receptors, and we realized that the EGF could not access the membrane area of the Xenopus oocytes other than at the very edge of the cells. This is probably due to the tight interaction, and therefore narrow space, between the oocyte membrane and the coverglass, which prevents the EGF molecules from diffusing efficiently into the region that is imaged. To circumvent this issue, we made a buffer solution containing 15 nM EGF and added this first to the empty imaging chamber. We then transferred the oocyte cells into the chamber and started imaging within two minutes. The results obtained in this way were quite different, and showed dramatic evidence for the effect of EGF on EGFR.

3.2 Addition of EGF induces linear motion of EGFR expressed in Xenopus oocytes

Unexpectedly, we observed linear tracks formed by fluorescence spots, which correspond to EGFR molecules (Figure 5A). This result is surprising, as we were expecting to see individual fluorescence spots, that would be photo-bleached in two-steps, as the canonical activation model of EGFR would have suggested.

A closer examination of these linear tracks reveals that they are composed of both stationary and mobile fluorescence spots (Figure 5B). In the same field of view, in addition to the linear tracks, there are also isolated small clumps of spots and seemingly single fluorescence spots. Unlike the stable fluorescent spots I observed when EGF is not present, the majority of the fluorescence spots are now mobile. These spots are either moving along the linear tracks or jiggling around their current positions. While I am not sure about the detailed mechanism behind the formation of these linear tracks, the addition of EGF to the oocytes has apparently increased the mobility of EGFR molecules on the oocytes membrane.

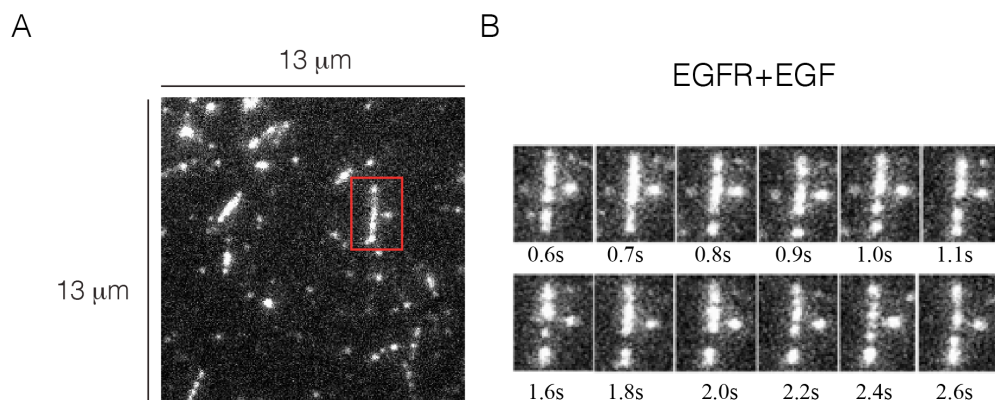


Figure 5 Linear motion of EGFR observed in the Xenopus oocytes, in the presence of EGF.

(A) TIRF image of a Xenopus oocyte expressing EGFR, after addition of 15 nM EGF. (B) Time-lapse images of the red rectangular area in A, showing the back-and-forth motion of EGFR molecules.

Unfortunately, the increased mobility of EGFR molecules presents a tremendous obstacle to the applicability of the stepwise photobleaching method. For the stepwise photobleaching method to work reliably, the fluorescent molecules need to be stationary enough throughout the period of photobleaching, so that the fluorescence intensities from the position of these molecules can be readily recorded and the events of photobleaching can be clearly identified during data analysis. Since the receptors can move in both the lateral and vertical direction (i.e., away from the plane of the coverglass), it is difficult to keep tracking the fluorescence intensity change of each individual spots. The lateral movement of the molecules could cause neighboring spots to transiently overlap, and later split away from each other. More importantly, in this live-cell based TIRF imaging process, the fluorescence intensity of each molecule fluctuates significantly as the distance between the plasma membrane and coverglass surface varies. As the EGFR molecule moves along the surface of the oocytes, which is not uniformly sticky to the glass surface, as I discuss later, the distance between the EGFR molecule and the glass surface constantly changes. Such vertical movements of the EGFR molecules lead to very large amount of fluctuation in fluorescence intensity traces. Even worse, because of the shallow depth of field being illuminated during the TIRF imaging, molecules could temporarily move out of the depth of TIRF illumination and then move back into it. Therefore, EGFR molecules can completely disappear from the field of view and show up at a different position seconds later. I therefore sought a strategy to stabilize these molecules in order for the stepwise photobleaching method to work.

I will return the analysis of EGFR stoichiometry in the presence of EGF in Chapter 4. In current Chapter, I will focus on the characterization of this unexpected linear motion of EGFR observed in Xenopus oocytes, in the presence of EGF.

3.3 Surface features of the Xenopus oocyte plasma membrane

As intrigued by this linear motion of EGFR as we were, a critical fact about the Xenopus oocyte membrane surface had been overlooked by us. It turns out that the plasma membrane of the Xenopus oocyte is not smooth or flat. Instead, as shown earlier by scanning electron microscopy (Sonnleitner et al., 2002), the plasma membrane of the Xenopus oocytes forms microvilli, which are essentially plasma membrane extrusions supported by actin based

cytoskeleton (Bretscher, 1983; Mukherjee and Williams, 1967; Sonnleitner et al., 2002). In other words, the plasma membrane of the *Xenopus* oocyte is far from being a plain two-dimensional lipid bilayer.

The size of the microvilli on the oocytes surface is about 1 μm in length and 100 nm in diameter (Sonnleitner et al., 2002). These dimensions match very well with that of the linear fluorescence intensity tracks observed in our experiment (Figure 6A). To further check if these linear tracks we observed are indeed somehow caused by these microvilli, we decided to fluorescently label the plasma membrane of oocytes and image the oocyte membrane using TIRF. We pre-incubated the oocytes with the Vybrant® CM-DiI Cell-Labeling reagent (Invitrogen) for 5 mins, and washed the oocytes a couple of times using the imaging buffer. With only the plasma membrane fluorescently labeled, we observed once again linear tracks that are very similar to what we saw when only EGFR is fluorescently labeled (Figure 6B). This result indicates that linear tracks formed by EGFR molecules in the presence of EGF are probably caused by the fact that these receptors are residing on the membrane of microvilli and therefore they are moving along and outlining the surface feature of the oocytes.

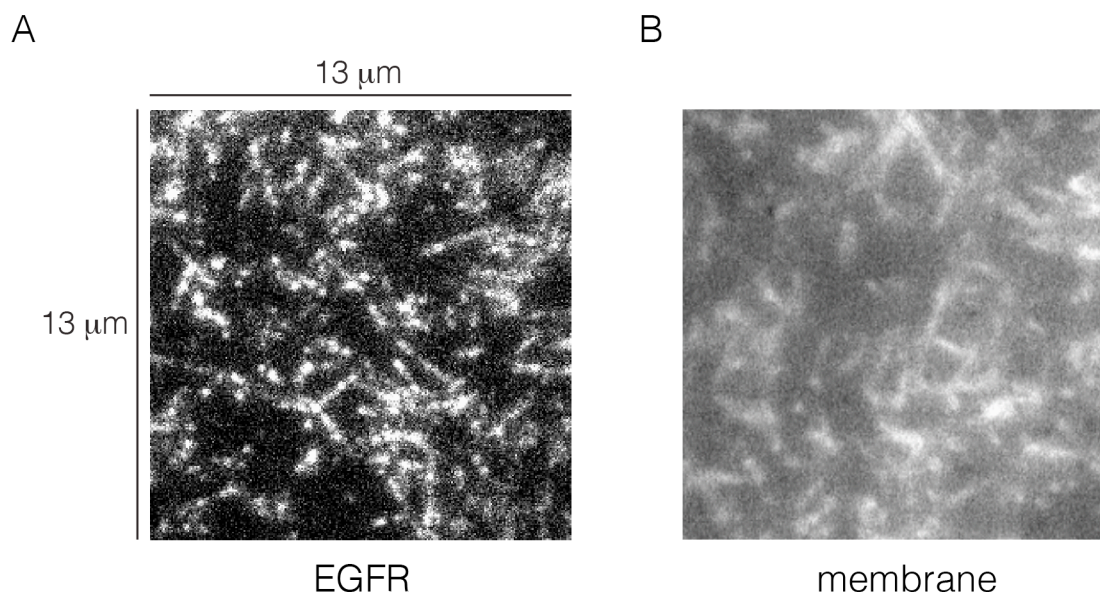


Figure 6 Comparison between TIRF images of EGFRs and the membrane on the *Xenopus* oocytes surface. (A) TIRF image of a *Xenopus* oocyte expressing GFP-tagged EGFR, in the presence of 15 nM EGF. (B) TIRF image of a *Xenopus* oocyte expressing EGFR without GFP tag, pretreated with plasma membrane labeling dye, in the presence of 15 nM EGF.

This observation reminds us that the plasma membrane is quite heterogeneous and is very different from an ideal uniform two-dimensional lipid bilayer sheet. One might think that such surface feature as the microvilli are somewhat unique to the *Xenopus* oocyte cells we used, but it turns out that the plasma membrane of mammalian cells is also rarely smooth and flat. For example, the human A431 cell line was visualized by scanning electron microscopy, using gold particles labeled with anti-EGFR antibody. The A431 cell line is a model human cell line used in studies of cancer-associated cell signaling pathways, because they overexpress EGFR. Strikingly similar to our observation with the *Xenopus* oocytes, gold particles appear to bind to the

microvilli and filopodia of the A431 cells, indicating the localization of EGFR molecules on these membrane extrusions from the cell surface (Heinzmann and Höfler, 1994).

3.4 EGFR activity and the actin cytoskeleton are required for linear motion of EGFR

Although we have established that the microvilli on the oocyte surface provide the morphological basis for the linear locomotion of EGFR (Figure 7A), we still do not understand the molecular basis behind this observation. Since the motion of EGFR was only triggered by the addition of EGF, we were motivated to investigate this further, hoping for a mechanistic understanding of this process. The results could potentially reveal new insights into the EGFR activation, as well as the interplay between the receptor and actin cytoskeleton.

We first mutated EGFR to inactivate the kinase domain (D813N), to test if the kinase activity of EGFR is required for this linear motion of the receptor. This catalytic inactive EGFR mutant does not form the linear tracks (Figure 7B). However, the majority of the EGFR D813N molecules are still “jiggling” and “blinking”. “Jiggling” means they are constantly moving back-and-forth laterally around their current positions. “Blinking” indicates they are also moving vertically, in and out of the illumination field of the excitation laser. Alternatively, for experiments using wild-type EGFR, if we pretreated the oocyte cells with 10 μ M of EGFR-specific kinase inhibitor PD153035 for 10 mins, we only observed the “jiggling” and “blinking” EGFR molecules, without seeing any linear tracks (Figure 7C). Together, these data indicate that the EGF binding to EGFR causes the receptor to become more mobile on the membrane, and that the kinase activity of EGFR is required for its motion along the microvilli.

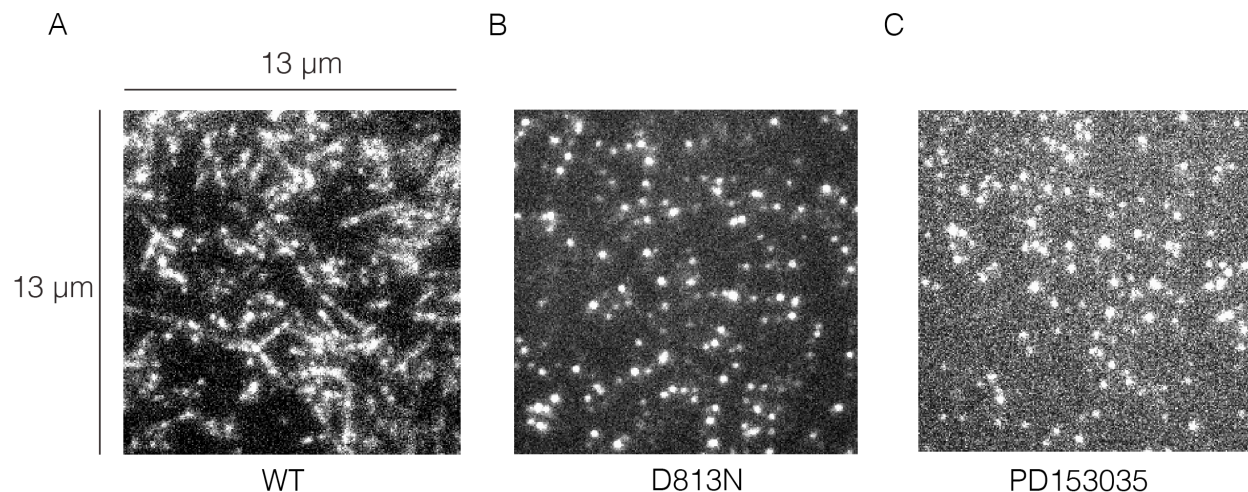


Figure 7 Effects of EGFR kinase activity on the linear motion of EGFR.

(A) TIRF image of a Xenopus oocyte expressing wild-type EGFR, in the presence of 15 nM EGF. This is the same as Figure 7A. (B) As in A, for a kinase dead EGFR mutant D813N. (C) As in A, the Xenopus oocyte was pretreated with 10 μ M PD153035 for 10 mins.

In searching for the potential mechanism of activated EGFR moving along the microvilli, one interesting earlier study from Donna J. Arndt-Jovin’s group caught our attention (Lidke et al., 2005). In that study, the authors used EGF coupled to quantum dots (QD-EGF) to indirectly

track EGFR on the A431 cell surface. They observed a directed retrograde transport of activated EGFR along the filopodia of cultured A431 cells. Briefly, the QD-EGF was added to the A431 cells and its movement was monitored by fluorescence microscopy. The QD-EGF initially bound near the tip of the filopodia, and then it started to move along the filopodia towards the cell body. Filopodia are structurally similar to microvilli. Both of them are membrane projections from the cell surface that are supported by actin microfilaments (Bretscher, 1983; Mattila and Lappalainen, 2008; Mukherjee and Williams, 1967). Filopodia are less stable than microvilli and they can turn into membrane ruffles or lamellipodia (Mattila and Lappalainen, 2008). The authors proposed a model to summarize their observations, in which the activated EGFR interacted with the actin microfilaments through the phosphorylated C-terminal tail regions and some unknown adaptor proteins. Once the linkage between the activated EGFR and actin microfilaments was generated inside the filopodia, the constant retrograde flow of the actin microfilaments drove the transport of activated EGFR molecules from the tip of the filopodia back to the cell body. By doing so, the cell could sense and react to signals received by receptors located distal to the main cell body, but within the reach of its filopodia.

The C-terminal tail region of EGFR carries tyrosine residues that are auto-phosphorylated upon the activation of EGFR. These phosphorylated tyrosine residues can then recruit adapter proteins and effector proteins to trigger various downstream signaling pathways. Interestingly, part of this C-terminal region (residues 984-996) has also been suggested to be able to bind actin directly, without phosphorylation (Hartigh et al., 1992). To test if the C-terminal region is involved in the linear motion of EGFR we observed, we expressed an EGFR mutant (Δ tail-2) in the oocytes, in which most of the C-terminal tail region (residues 965-1186) was deleted. Upon the addition of EGF, this tail-less EGFR construct (Δ tail-2) shows robust formation of linear tracks (Figure 8A). This indicates that the C-terminal tail region is unlikely to be required for the linear motion of EGFR. This is contradictory to the idea that C-terminal tail phosphorylation of EGFR is mediating the motion, through either direct or indirect interaction with the actin cytoskeleton. Thus, the mechanism behind our observation may be different from that behind what Arndt-Jovin's group has described in their work, although they have not tested whether the C-terminal tail is indeed required for the phenomenon they described. Another apparent difference between their observations and ours is the direction of the EGFR motion. In their study, activated EGFR-EGF complexes moved from the tip of filopodia towards the A431 cell body. Since the motion of EGFR is from the plus end to the minus end of the actin microfilaments, the authors described the motion as "directed retrograde transport". In our experiments, EGFR molecules are constantly changing the direction and speed of their motion. Unfortunately, because the EGFR molecules are jiggling and blinking, it is very difficult to reliably track individual spots for long enough time, in order for us to extract useful quantitative information about their velocities. Based on the results, we can only conclude that the motion is not unidirectional and the speed varies.

If we pretreated the oocytes with 1 μ M latrunculin B, a potent actin inhibitor that sequesters G-actin and prevents F-actin assembly, we could no longer observe the linear motion of EGFR along microvilli (Figure 8B). This result strongly suggests that the actin cytoskeleton is critical in this process. There are at least two types of actin-based cytoskeleton that could be involved in supporting the motion of EGFR along the microvilli, actin microfilaments (Kwiatkowska et al., 1991; Rijken et al., 1991) and the cortical actin meshwork (Kapus and Janmey, 2013; Ritchie et al., 2003). Inhibition of F-actin assembly by latrunculin B could disintegrate the actin microfilaments inside the microvilli. Alternatively, latrunculin B could also

affect the integrity of the cortical actin meshwork just underneath the plasma membrane. Both of the scenarios could potentially cause the collapse of unsupported microvilli back onto the oocytes surface, as suggested by previous studies (Runge et al., 2007).

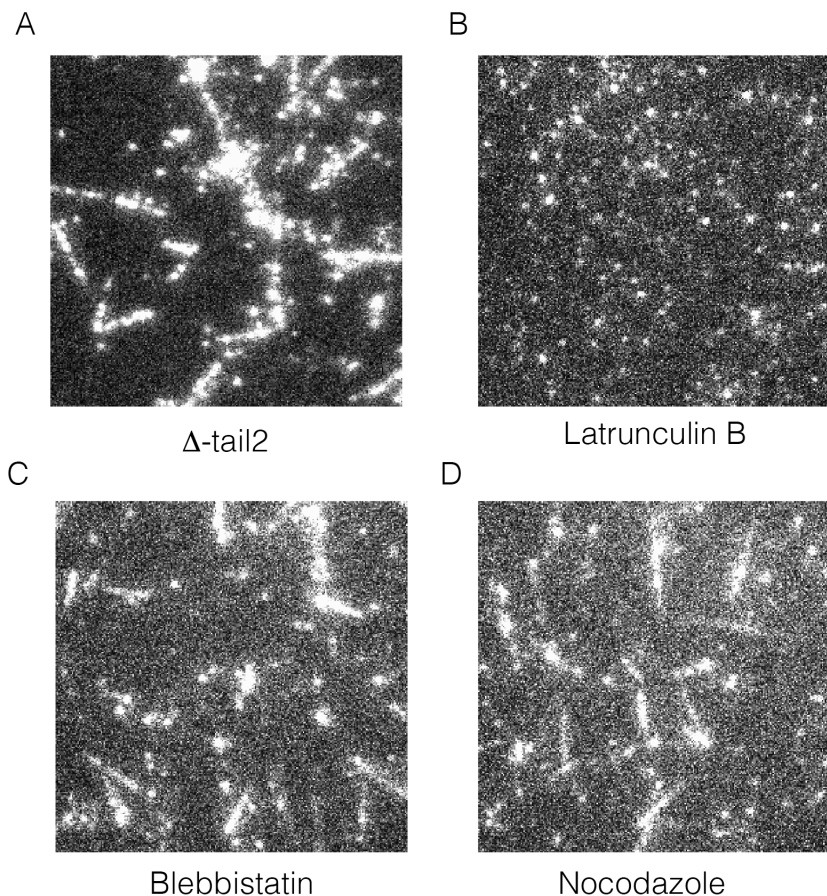


Figure 8 Effects of EGFR C-terminal tail and cytoskeleton on the linear motion of EGFR.

(A) TIRF image of a Xenopus oocyte expressing EGFR Δ -tail2 mutant, deletion of the entire C-terminal tail (residues 965 to 1186), in the presence of 15 nM EGF. (B)(C)(D) TIRF images of a Xenopus oocyte expressing wild-type EGFR, in the presence of 15 nM EGF. Oocytes are pretreated with (B) 1 μ M latrunculin B for 5 mins, (C) 10 μ M blebbistatin for 10 mins and (D) 50 μ M nocodazole for 30 mins.

Myosins are the actin-based motor molecules that can interact with actin filaments and cargo proteins simultaneously. To test if a myosin could play a “bridging” role to mediate EGFR motion along the microvilli, we pretreated the cells for 10 mins with 10 μ M blebbistatin, which is the only myosin inhibitor that was commercially available at the time. We did not observe any difference between blebbistatin-treated and non-treated oocyte cells, regarding the formation of linear tracks by EGFR (Figure 8C). Unfortunately, blebbistatin appears to be a selective inhibitor for Myosin II, which is the myosin type responsible for muscle contraction. This result indicates that the Myosin II is not involved in our observation. However, we could not rule out the possibility of other types of myosin being involved. One particular interesting type is Myosin VI, which is an unconventional myosin in the sense that it travels along the actin filaments from plus end to minus end (Roberts et al., 2004). Myosin VI has been reported to be involved in the

retrograde transport of endocytic vesicles along actin microfilaments into the cells (Hasson, 2003).

Since microtubules form the other type of cytoskeleton that could support linear motion and intracellular trafficking of cargo proteins, we also tested if microtubules were involved in the linear motion of EGFR. We pretreated the cells for 30 mins with 50 μ M nocodazole, which inhibits microtubule polymerization. The result shows that the EGFR can still form the linear tracks after the pretreatment with Nocodazole (Figure 8D), confirming that microtubules are unlikely to be involved in this process. This is not very surprising, since there is no evidence for the existence of microtubules inside the microvilli (Bretscher, 1983).

Summary

Although the observation about the linear motion of EGFR along the microvilli is really unexpected and intriguing to us, we have yet to reach a coherent understanding of this phenomenon. Before we can fully uncover the molecular details and the mechanism of this observation, more thorough studies and analysis are necessary. Meanwhile, this observation represents a major challenge for us to extract the information on EGFR stoichiometry in the presence of EGF. In order to apply the stepwise photobleaching counting method for the analysis of EGFR stoichiometry in the presence of EGF, we developed a strategy to stop the motion of EGFR and make the receptors more stable.

Chapter 4 Analysis of the stoichiometry of human EGFR expressed in *Xenopus* oocytes in the presence of EGF

Introduction

In this Chapter, I describe the strategy that successfully limits the motion of EGFR and enables us to determine the stoichiometry of EGFR after activation. We found that EGFR forms dimers and multimers in the presence of EGF. Various potential interfaces were tested for their contribution to EGFR multimerization and we identified a cluster of residues in Domain IV that are specifically important for multimerization of EGFR.

4.1 FLAG-tag helps in stabilizing the EGFR molecules expressed in *Xenopus* oocytes in the presence of EGF

To stabilize the EGFR molecules on the *Xenopus* oocyte membrane after the addition of EGF, one idea came to mind is to somehow “grab” the receptors and stop their motion. Inspired by some pioneering work in the field of single-molecule biophysics, in which others have studied proteins and protein complexes in vitro at the single-molecule level (Jain et al., 2011; Yildiz et al., 2004), we explored the strategy of immobilizing an antibody on the coverglass, which can in turn bind to the extracellular part of EGFR, to hold the receptor stationary. Unfortunately, most known antibodies to the EGFR extracellular domain are antagonists of the receptor. Consequently, the binding of these antibodies to the extracellular domain of EGFR will either interfere with the ligand-receptor interaction, or result in extracellular domain conformations that are not compatible with the formation of ligand-induced extracellular dimer.

To avoid interference with the ligand-receptor interaction and the subsequent receptor conformational change, we decided to add a FLAG-tag (DYKDDDDK) to the N-terminus of EGFR on the extracellular domain. By doing so, we could abandon the use of anti-EGFR antibodies. Instead, now we only need to immobilize the anti-FLAG antibodies on the coverglass surface and use them to hold FLAG-tagged EGFR molecules stationary. Importantly, addition of FLAG tag to the N-terminus of EGFR does not seem to affect its normal function (Jura et al., 2009b; Zhang et al., 2006).

Quite unexpectedly, once we expressed this FLAG-tagged EGFR in the *Xenopus* oocytes, we observed a significant reduction in the mobility of EGFR molecules, after EGF addition but without using antibodies. This is the effect that we were hoping for, but we did not expect the FLAG-tagged EGFR to become stationary with no anti-FLAG antibody on the glass surface. Presumably, there is fortuitous adherence between the FLAG tag and the coverglass that immobilizes the receptors. We verified that the FLAG-tagged EGFR still exhibits predominantly single-step photobleaching in the absence of EGF.

Luckily, now that we have managed to reduce the mobility of EGFR molecules after their binding to EGF, and the stepwise photobleaching counting method can be applied again. In Chapter 2 and 3, the EGFR used for analysis is without the FLAG tag. For simplicity, I will refer the “FLAG-tagged EGFR” as “EGFR” in the following discussion in this chapter.

4.2 Addition of EGF to EGFR generates dimers and higher-order multimers

We added EGF at 15 nM concentration to *Xenopus* oocytes expressing EGFR. The EGF was added to cells in suspension, before they were placed on the microscope slide, since the surface of the cell that interacts tightly with the glass is inaccessible to EGF. The EGF concentration is 8-fold higher than the measured IC-50 value of 1.9 nM for EGF binding to EGFR in a competition assay (Jones et al., 1999). We monitored photobleaching within 2 minutes of EGF addition, which minimizes the effects of receptor internalization. With the addition of EGF, We observed two-step photobleaching for some spots, as well as multi-step photobleaching (three or more steps) for nearly half of the spots (Figure 9A, B). As can be seen by comparing Figures 2B and 9A, the addition of EGF results in the appearance of some particularly bright spots that are also irregular in shape. We excluded such spots from the analysis.

We grouped all spots for which there are more than two-steps in the photobleaching trace into one category, referred to as multi-step bleaching. Roughly 50% of the spots show multi-step bleaching, ~25% show two-step bleaching and ~25% show one-step bleaching (Figure 9B). We analyzed photobleaching data for an EGFR variant in which the catalytic base is mutated (D813N). This kinase-dead variant of EGFR exhibits a similar degree of multimerization to wild-type EGFR, demonstrating that the formation of multimers does not require signaling from active kinases (Figure 9C).

We repeated the step-wise photobleaching experiments using TGF- α as the ligand instead of EGF, and found a similar distribution of one-step, two-step and multi-step photobleaching events (Figure 9D). Although the structure of EGF is very similar to that of TGF- α , the residues that are surface exposed when EGF is bound to EGFR are not conserved in TGF- α (Garrett et al., 2002; Ogiso et al., 2002). We conclude that neither EGF nor TGF- α is likely to be at the interfaces between protomers in the multimers. The binding of EGF to EGFR exhibits negative cooperativity, which has been interpreted in terms of half-site binding of EGFR to EGF (i.e., at a stoichiometric ratio of 2:1) at low ligand concentrations (Alvarado et al., 2010; Arkhipov et al., 2013b; Liu et al., 2012; Pike, 2012). We analyzed step-wise photobleaching events upon addition of 2 μ M EGF, instead of the 15 nM used in most of the experiments we reported. This 133-fold increase in ligand concentration did not lead to a substantial difference in the relative population of multimers, indicating that the multimer interface does not involve empty ligand binding sites (Figure 9E).

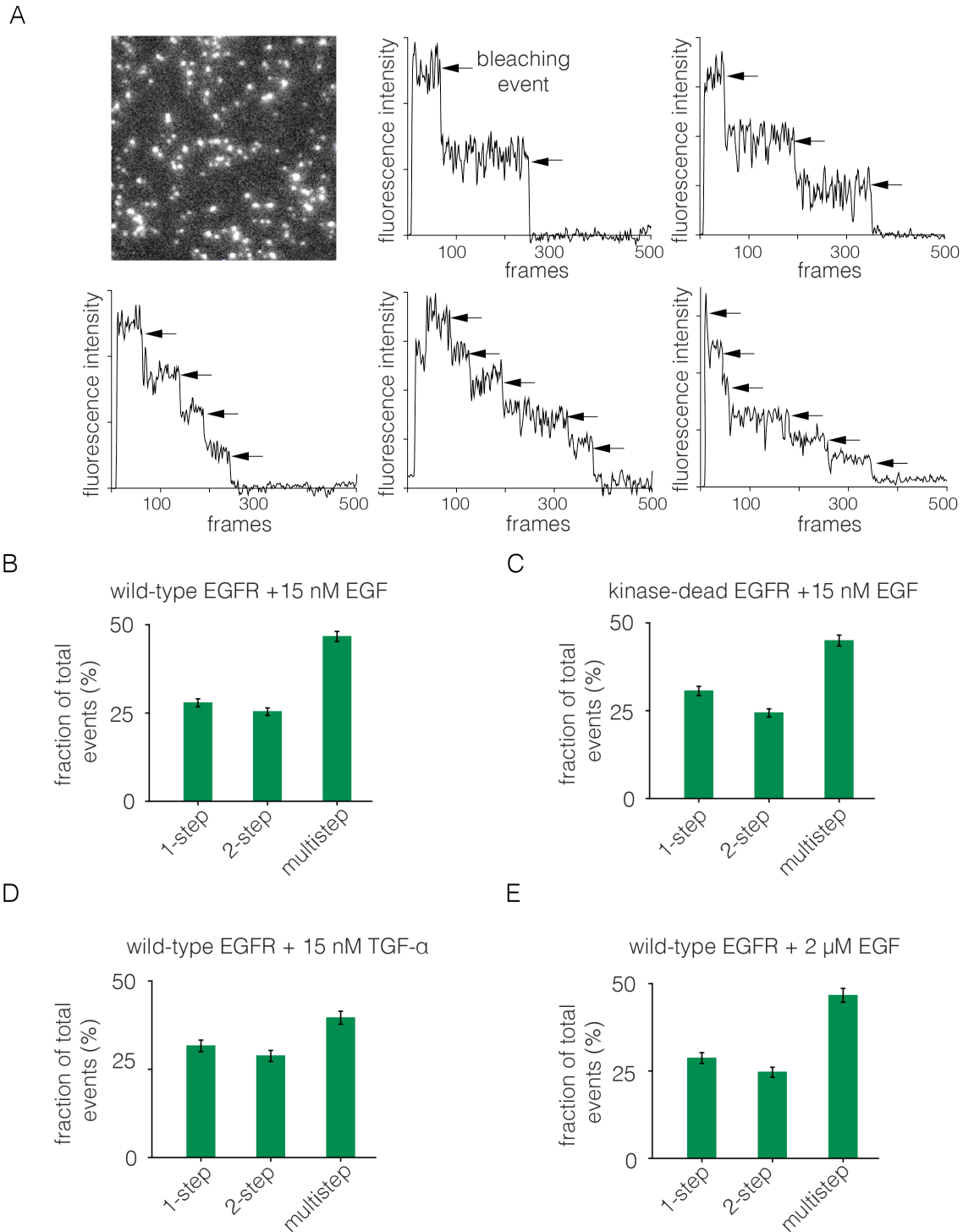


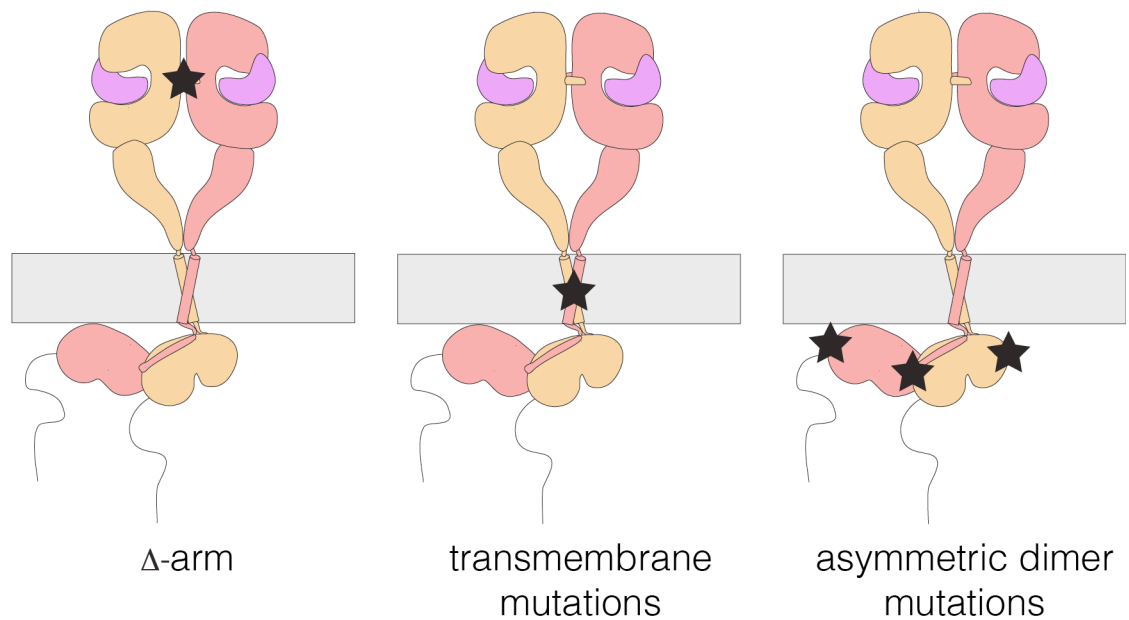
Figure 9 Analysis of photobleaching events for EGFR in the presence of EGF.

(A) TIRF image of a *Xenopus* oocyte expressing EGFR, 2 mins after addition of 15 nM EGF. Five representative photobleaching traces are shown, in which two to six photobleaching events can be identified. Traces with more than two steps are denoted “multi-step”. (B) Histogram showing the fraction of one-step, two-step and multi-step photobleaching events for wild-type EGFR in the presence of 15nM EGF. (C) As in B, for a kinase-dead mutant of EGFR (D813N). (D) As in B, for TGF- α as the ligand, at a concentration of 15 nM. (E) As in B, but for a 133-fold higher concentration of EGF (2 μ M). (Adapted from eLife 2016;5:e14107)

4.3 Analysis of the role of the dimer interface in EGFR multimerization

We made mutations that are expected, separately, to disrupt the dimerization of the extracellular module, the transmembrane helices, and the kinase domains. We deleted the dimerization arm in the extracellular module (Δ -arm) and found that the extent of multimerization was not affected substantially (Figure 10). Deletion of the dimerization arm has both positive and negative effects on the receptor dimerization, as noted earlier, which might account for the neutral effect of this deletion on multimerization. We disrupted both the N- and C-terminal dimerization interfaces of the transmembrane helix (Arkhipov et al., 2013a; Endres et al., 2013; Fleishman et al., 2002), by replacing Thr 624, Gly 625, Gly 628, Gly 629, Ala 637 and Gly 641 simultaneously by isoleucine (Endres et al., 2013). To disrupt the asymmetric dimer interface in kinase domains, we introduced two mutations (I682Q, V924R) (Zhang et al., 2006). Both sets of mutations resulted in substantial reduction in the extent of multimerization (Figure 10).

A



B

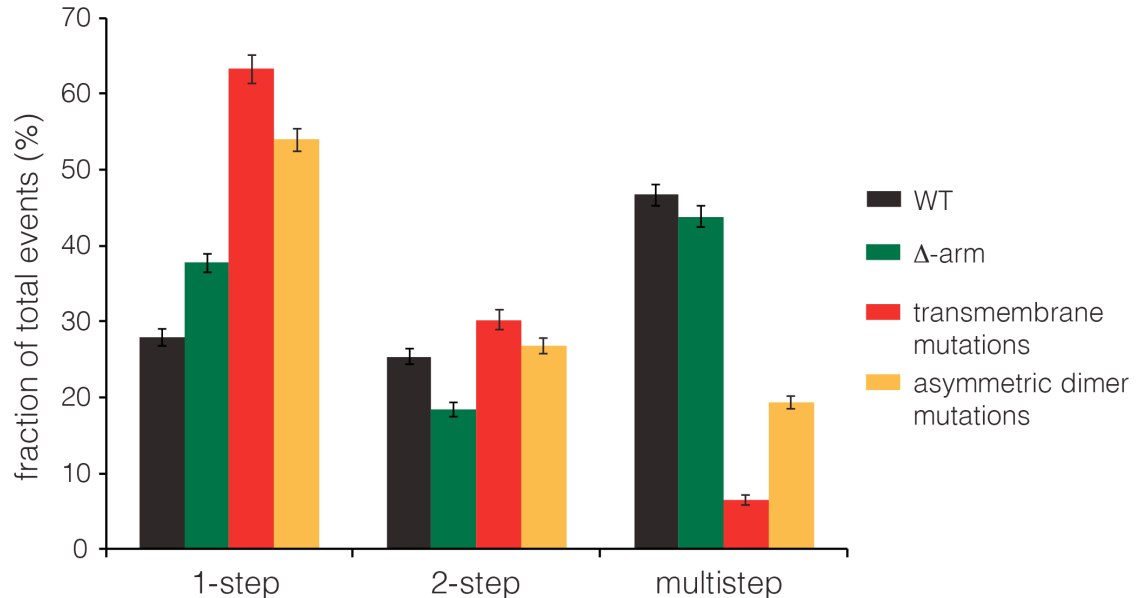


Figure 10 Effects on multimerization of mutations in EGFR that also affect dimerization.

(A) Schematic diagram showing the locations of mutations with respect to the EGFR dimer. Δ -arm, deletion of the dimerization arm of the extracellular module. TM, mutations in the transmembrane helix (Thr 624, Gly 625, Gly 628, Gly 629, Ala 637 and Gly 641 are all replaced by isoleucine). Asymmetric dimer interface mutations combine the mutations I682Q in the N-lobe and V924R in the C-lobe of the kinase domain. (B) Histogram showing the fraction of one-step, two-step and multi-step photobleaching events in *Xenopus* oocytes for wild-type and mutant EGFRs. (Adapted from eLife 2016;5:e14107)

We wondered if the transmembrane helices alone could be responsible for multimerization, perhaps by forming separate cross-bridges through the N-terminal and C-terminal dimerization elements. To test this, we made a construct in which the transmembrane helix of EGFR was fused to mCherry at the N-terminus and EGFP at the C-terminus. This construct was studied by photobleaching, and it exhibited one-step and two-step photobleaching, with no evidence for multistep photobleaching (Figure 11). We conclude that the transmembrane helices do not form multimers by themselves at the low expression levels used in our experiments. An interesting aspect of these data is that the extent of dimerization for the isolated transmembrane helices (~13%) is greater than that seen for full-length EGFR (~3%) without EGF (compare Figures 11 and Figure 3A). This is consistent with the idea that the tethered conformation of the ligand-free extracellular domain blocks receptor dimerization.

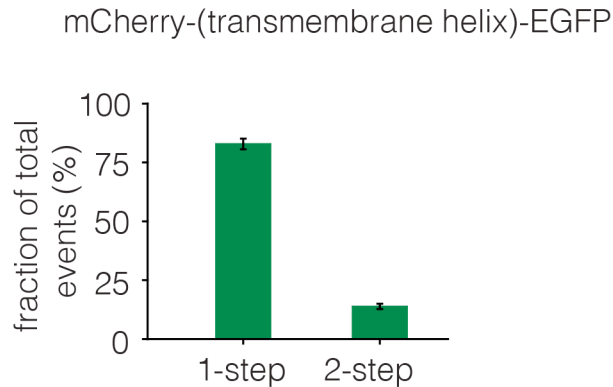


Figure 11 Dimerization of the isolated transmembrane helix, in the absence of EGF.

The EGFR transmembrane helix was fused to mCherry at the N-terminus and to EGFP at the C-terminus. The fraction of one-step and two-step photobleaching events of EGFP in *Xenopus* oocytes is shown for this construct. No multi-step photobleaching events were observed. (Adapted from *eLife* 2016;5:e14107)

4.4 Identification of residues in Domain IV that are necessary for EGFR multimerization

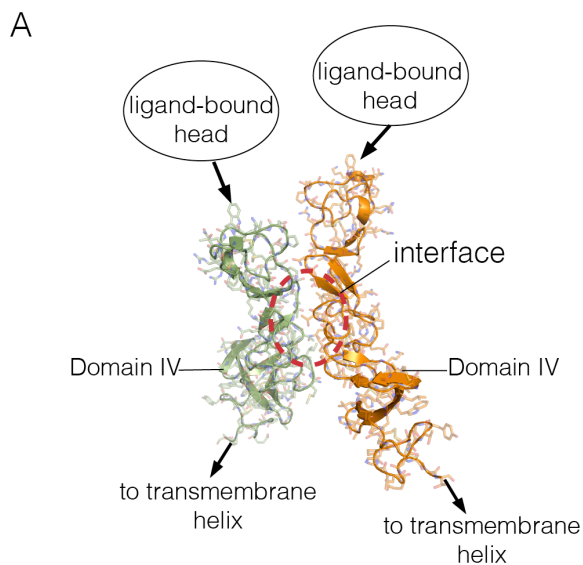
It is difficult to separate the structural requirements for multimerization from those necessary for dimerization. We wondered whether the extracellular domain has an interface that is required for multimerization, but not for dimerization or ligand binding. Packing interactions in crystal structures of the extracellular domains of EGFR family members do not provide obvious clues concerning such an interface. We therefore turned to computational docking to see if there are ways in which the extracellular domains might self-associate.

In collaboration with Deepti Karandur, a postdoc in Kuriyan lab, we first ran the docking program ClusPro, which emphasizes shape complementarity between protomers in generating models for protein complexes (Kozakov et al., 2013), using the structures of the entire dimeric extracellular module (PDB code: 3NJP) or a dimer containing just the ligand-bound head (PDB code: 1MOX), with no constraints. This led to docking solutions that were either physically implausible (i.e., the two dimers of the extracellular module could not be connected to the same membrane), or that had EGF at the interface between dimers. Since our experiments made it unlikely that EGF bridges EGFR dimers in a multimer, we concluded that ClusPro is unable to provide plausible models for self-interaction, which we expect to be very weak in the absence of organization on the membrane.

We then ran ClusPro using a single copy of the structure of the Domain IV leg alone. Although this did not result in one clear solution, we were intrigued by a family of solutions in which one face of Domain IV was packed upon itself in a dimer (Figure 12A). These solutions have a surface containing several hydrophobic residues at the interface between two Domain IV molecules (Figure 12B). This surface is not involved in formation of the EGF-bound EGFR dimer, and it is distal to the surface of Domain IV that forms the tethering interaction in autoinhibited ligand-free EGFR. This surface region therefore represents a potential interface for formation of a multimer of dimers.

There are three isoleucine residues in this surface region (residues 545, 556, 562) and one valine residue (Val 592) (Figure 12B, left). We first made two quadruple mutations, in which

both I545 and I556 were replaced by either lysine or alanine, while I562 and V592 were mutated to arginine and glutamate, respectively. The variant harboring mutations I545K, I556K, I562R and V592E (denoted “IIIV/KKRE”) shows significant reduction of multimerization (Figure 12C). In contrast, the variant with I545A, I556A, I562R and V592E (“IIIV/AARE”), shows a similar extent of multimerization as wild-type EGFR (Figure 12C). I discuss in next chapter the effect of these mutations on the activity of the receptor. We found that the effect on EGFR activity of a double mutation (I545K and I556K; “II/KK”) is similar to that of the IIIV/KKRE quadruple mutation (not shown). We concluded that Ile 545 and Ile 556, which are further from the membrane and closer to Domain III, are important for multimerization, whereas the residues that are closer to the membrane, Ile 562 and Val 592, are not. We replaced three residues in the membrane-distal region of the predicted interaction surface, Val 526, Glu 527 and Asn 528, by glutamate, arginine and arginine, respectively (“VEN/ERR”; Figure 12B, right). In another variant we replaced Thr 548 and Asn 554 by arginines (“TN/RR”; Figure 14B, right). Both of these variants also show reduced multimerization (Figure 12C). Taken together, these data suggest that the residues in Domain IV shown in Figure 14B, spanning residues 526 to 556, are involved in multimerization of the receptor. We note that we have tested only a limited set of mutations, and that therefore our list of residues within a putative interfacial region is likely to be incomplete.



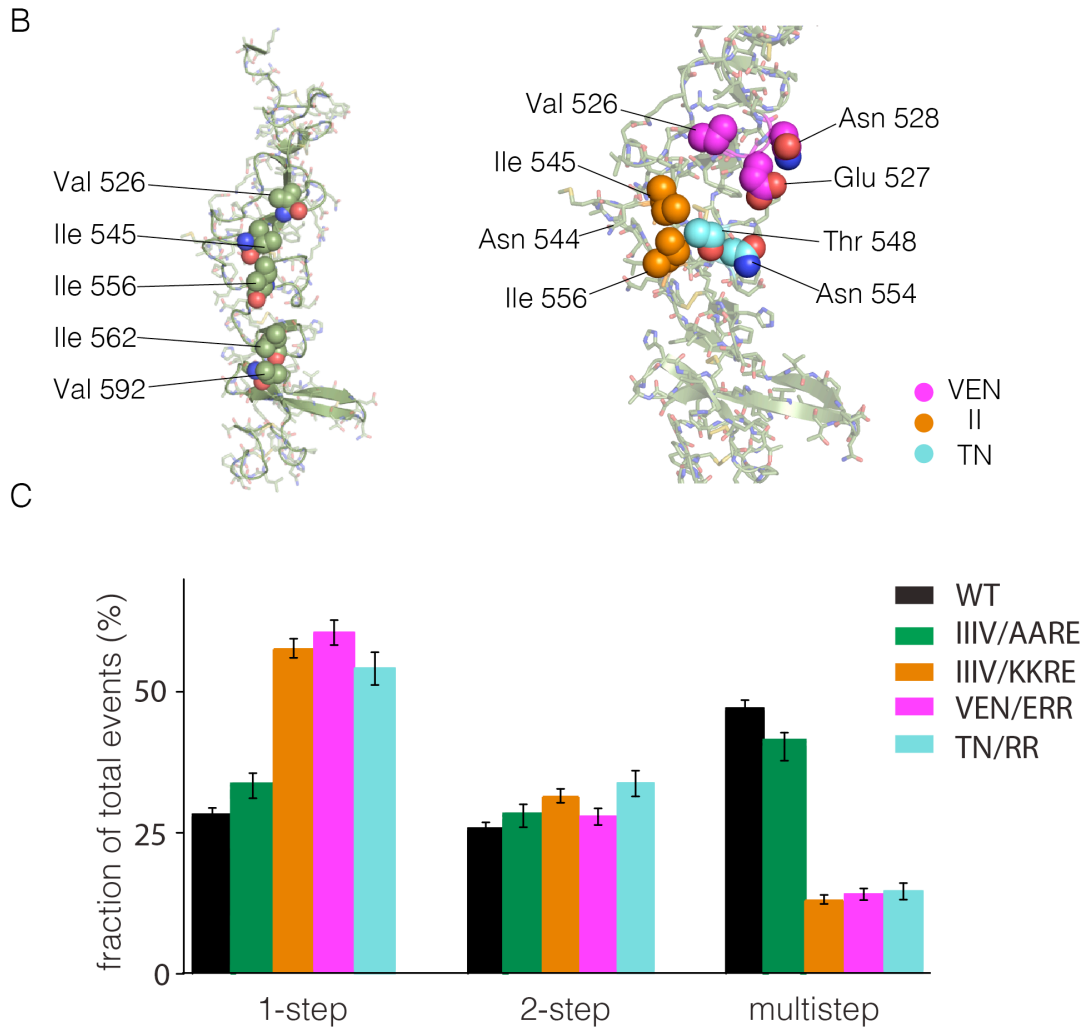


Figure 12 Identification of a possible interface between the Domain IV legs of two EGFR molecules.

(A) A representative dimer generated by ClusPro from a docking calculation done using a single isolated Domain IV. The interface between the two domains is not involved in dimerization, and is on the opposite face of the domain with respect to the interface involved in autoinhibitory tethering. (B) Residues on Domain IV that were mutated to examine their effects on multimerization and activity. (C) Histogram of the fractions of one-step, two-step and multi-step photobleaching events in *Xenopus* oocytes for wild-type and mutant EGFR. IIIV/AARE: I545A, I556A, I562R and V592E. IIIV/KKRE: I545K, I556K, I562R and V592E. VEN/ERR: V526E, E527R and N528R. TN/RR: T548R and N554R. (Adapted from eLife 2016;5:e14107)

Summary

In the presence of EGF, we found that ligand-induced receptor self-association does not end at dimerization, but it continues with the generation of multimers. While the existence of such higher-order assemblies of EGFR has been reported before, their structure and function are largely unknown. We found that dimerization interfaces of EGFR, except the dimerization arm region in the extracellular domain, also play important role in receptor multimerization. More importantly, we identified a cluster of residues in Domain IV of EGFR that specifically affect receptor multimerization rather than dimerization. These residues provide us a powerful tool to uncover the functional role of multimerization in EGFR activation.

Chapter 5 Functional role of multimerization in EGFR activation

Introduction

In this Chapter, I utilize the mutations that are specifically important for EGFR multimerization, to examine the functional role of multimerization in EGFR activation and signaling. EGFR autophosphorylation and the phosphorylation of two downstream signaling proteins were analyzed. The analysis suggests that EGFR multimerization is particularly important for the phosphorylation of PI3K, which is reported to bind to a proximal tyrosine site on the EGFR C-terminal tail. I also learnt from the analysis that EGFR multimerization could be critical for efficient autophosphorylation of proximal tyrosine sites. Based on our experimental observations, we propose a structural model for EGFR multimerization.

5.1 Effects of Domain IV mutations on EGFR tail phosphorylation

The multimerization of EGFR has been reported before, and it has been noted that the formation of tetramers is correlated with the recruitment of the adapter protein GRB2 (Clayton et al., 2005, 2008; Kozer et al., 2013, 2014). Nevertheless, a functional role for ligand-dependent multimerization has yet to be established definitively. The mutations that we have identified in Domain IV of EGFR that block multimerization, but not dimerization, provide an opportunity to identify the effects of multimerization on EGFR function. To test the effect of these mutations on the activity of EGFR, I used transient transfection in mammalian cells (HEK293T), followed by measurement of phosphorylation on EGFR and downstream signaling effector proteins by FACS assay, as described (Kovacs et al., 2015b). I monitored one proximal site in the EGFR C-terminal tail, Tyr 992, and one distal site, Tyr 1173 (antibodies with minimal cross-reactivity are available for these sites, see (Kovacs et al., 2015b)).

I compared autophosphorylation of wild-type EGFR with that of three variants with mutations in Domain IV (II/KK; VEN/ERR; TN/RR; see Figure 12B for the positions of the mutated residues). Figure 13 shows the phosphorylation levels for Tyr 992, the proximal site, and Tyr 1173, the distal site, for wild-type EGFR and the mutants at an intermediate level of expression in the FACS assay. Each of three mutants show reduced phosphorylation of both sites compared to wild-type. For example, for the II/KK mutant, phosphorylation of Tyr 992 and Tyr 1173 are reduced to ~35% and ~50% of the wild-type levels.

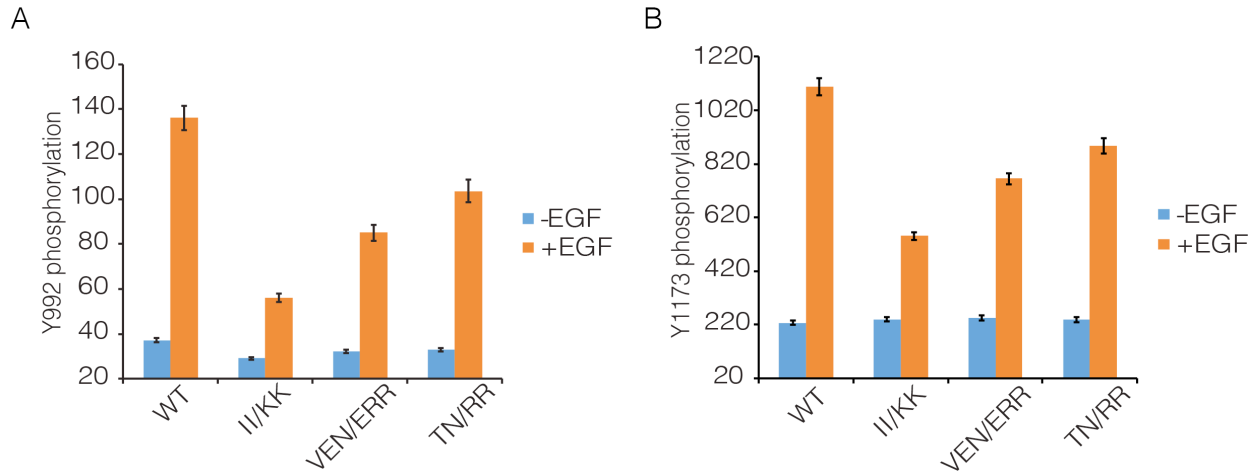


Figure 13 Effect of Domain IV mutations on phosphorylation of EGFR.

Wild-type (WT) or mutant EGFR was transfected into HEK293T cells, and phosphorylation was measured using FACS. The EGFR mutants are: II/KK (I545K, I556K); VEN/ERR (V526E, E527R and N528R); TN/RR (T548R and N554R). (A) Phosphorylation of a proximal site (Tyr 992) in EGFR. The bar graph shows the average phosphorylation level from cells expressing an intermediate level of EGFR, selected based on the whole range of EGFR expression in the FACS analysis, with (orange) and without (blue) the addition of EGF. (B) As in Panel A, for a distal site (Tyr 1173) in EGFR. (Adapted from eLife 2016;5:e14107)

Sean Peterson, a postdoc in our group, verified that the surface expression of EGFR is not affected by mutations in Domain IV. To do this Peterson made a construct in which an HA epitope tag is fused to the N-terminus of EGFR, with a fluorescent protein (Venus) fused to the C-terminus. This construct was transiently transfected into HEK293T cells, as for the activity assays shown above. An HA-specific antibody was used to visualize surface-exposed EGFR in individual cells using a fluorescence microscope, and the total expression of EGFR was monitored by detecting fluorescence of the Venus protein tag. As shown in Figure 14, there is no difference in the ratio of surface-exposed to total EGFR for wild-type compared to the II/KK mutant, over the entire range of EGFR expression in the experiment.

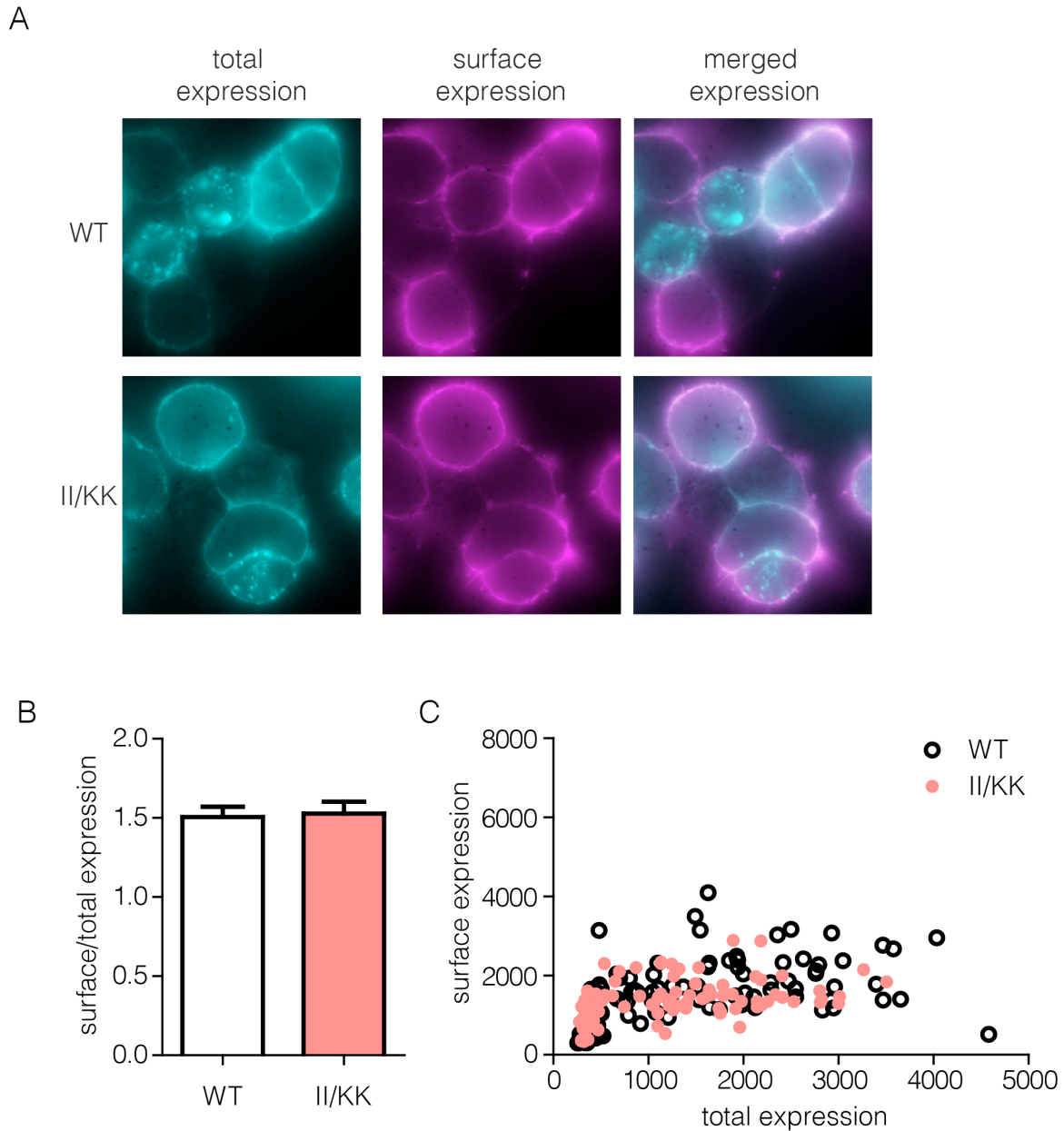


Figure 14 Surface expression of wild-type EGFR and II/KK mutant.

(A) Total receptor (cyan) show some intracellular stores of receptor but very efficient trafficking of wild-type and II/KK (I545K/I556K) EGFR to the cell surface (magenta). (B) Quantification of surface/total ratio of approximately 100 cells from three independent experiments (error bars are SEM from N=3). The ratio is calculated from integrated fluorescence intensity values from each channels. (C) Representative data from one independent experiment show plot of raw total versus surface values. Each point is a region of interest (ROI), which is roughly equivalent to one cell. (Adapted from eLife 2016;5:e14107)

I note that one of the glycosylation sites in EGFR, Asn 544 (Zhen et al., 2003), is located close to residues Ile 545 and Ile 556 (see Figure 12B). I wondered whether mutations in Domain IV could be affecting this glycosylation site, and perhaps altering multimerization and signaling in that way. I made two EGFR variants in which Asn 544 was replaced by either aspartate or

glutamine. Both mutant receptors show negligible reduction in EGFR tail phosphorylation (Figure 15).

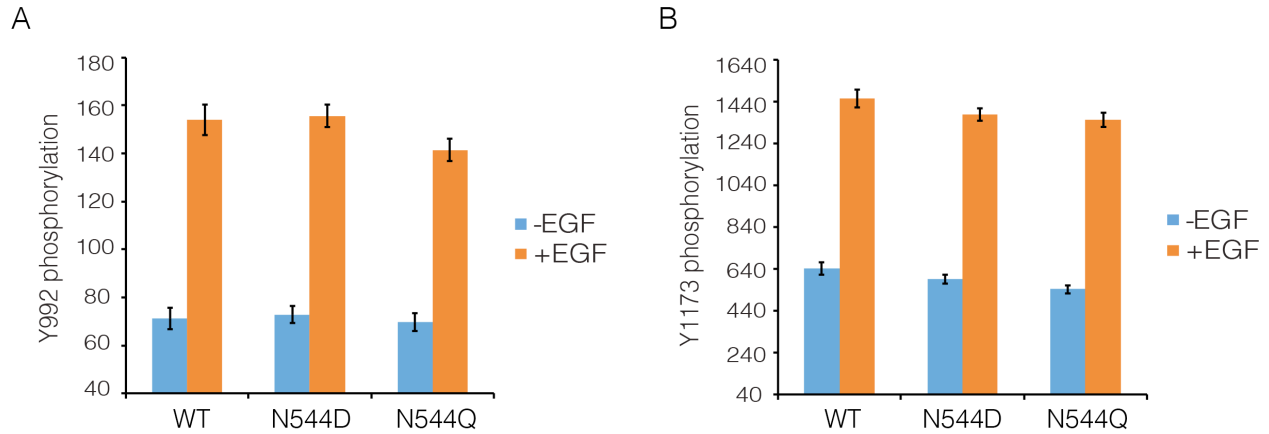


Figure 15 Effect of Asn 544 mutations on phosphorylation of EGFR.

Wild-type (WT) or mutant EGFR with Asn 544 replaced by Asp (N544D) or Gln (N544Q) was transfected into HEK293T cells, and phosphorylation was measured using FACS. (A) Phosphorylation of a proximal site (Tyr 992) in EGFR. The bar graph shows the average phosphorylation level from cells expressing an intermediate level of EGFR, selected based on the whole range of EGFR expression in the FACS analysis, with (orange) and without (blue) the addition of EGF. (B) As in Panel A, for a distal site (Tyr 1173) in EGFR.

5.2 Effects of Domain IV mutations on two effector proteins

I also monitored the phosphorylation of two proteins that are expected to be activated as a consequence of distal and proximal phosphorylation of the EGFR tail, respectively. Extracellular signal-related kinase (ERK) is activated by distal phosphorylation of EGFR, through the docking of the adapter proteins GRB2 and SHC (Batzer et al., 1994). Signaling from proximal sites in EGFR is less well characterized than for distal sites, but a comprehensive study of EGFR phosphopeptides binding to other proteins showed that the SH2 domains of the α and β isoforms of phosphatidylinositol 3-kinase (PI3K), and that of phospholipase C- γ , bind with high affinity only to sites in the proximal segment of the EGFR tail (Jones et al., 2006). I monitored PI3K, and found that mutations in Domain IV result in attenuation of PI3K phosphorylation, to ~30% of the wild-type level (Figure 16A). In contrast, the phosphorylation of ERK by the MAP-kinase pathway is not affected by Domain IV mutations (Figure 16B).

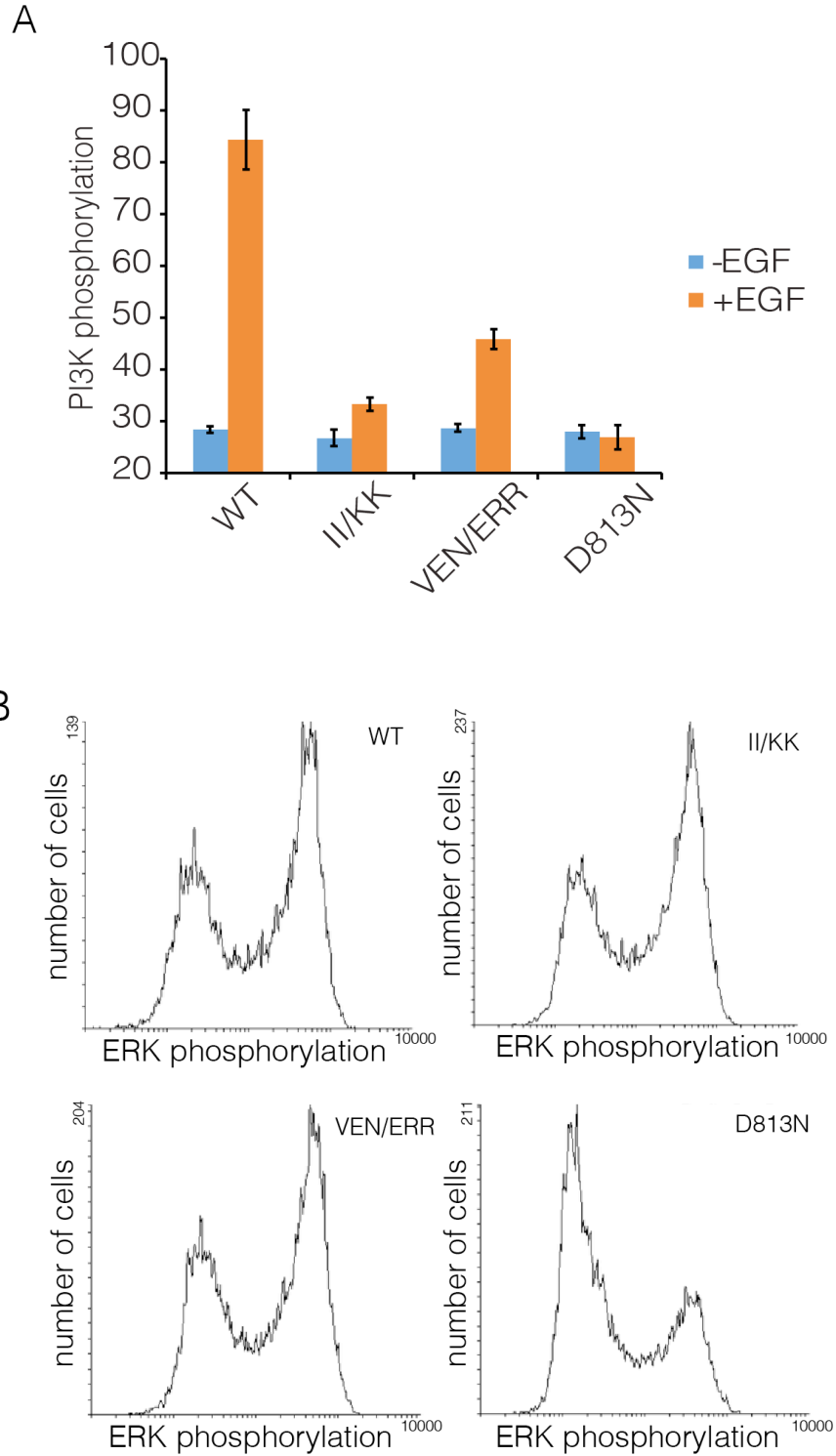


Figure 16 Effect of Domain IV mutations on phosphorylation two effector proteins.

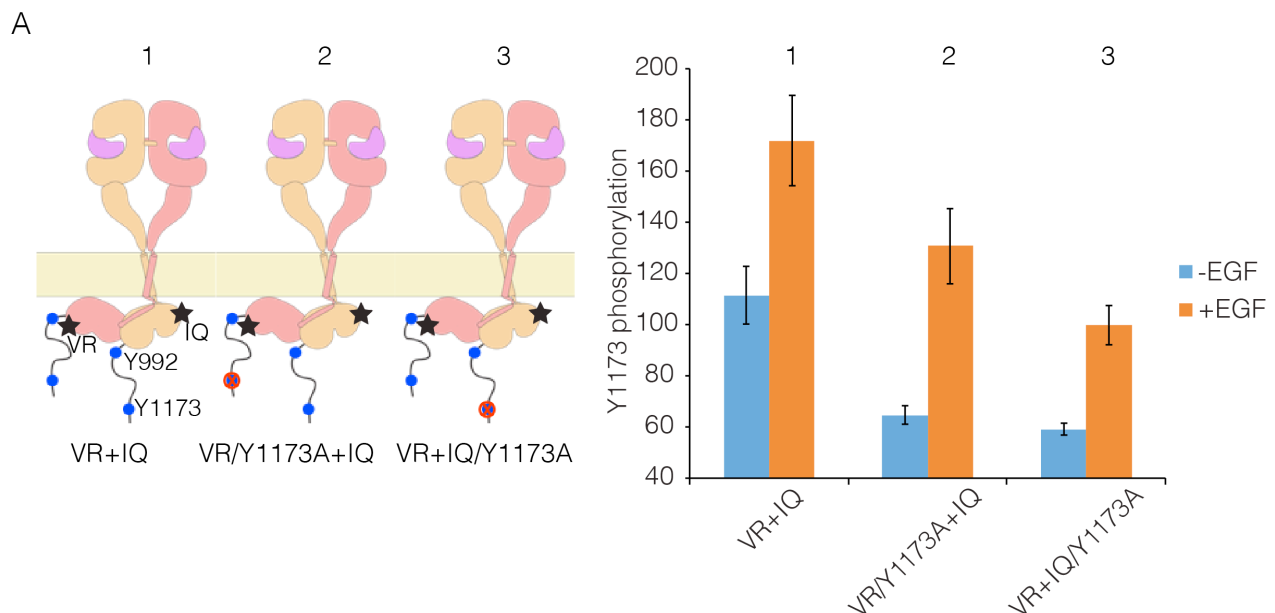
Wild-type (WT) or mutant EGFR was transfected into HEK293T cells, and phosphorylation was measured using FACS. The EGFR mutants are: II/KK (I545K, I556K); VEN/ERR (V526E, E527R and N528R); TN/RR (T548R and N554R). (A) As in figure 15, for phosphorylation of PI3K. In addition to two mutations in Domain IV (II/KK and VEN/ERR), the phosphorylation levels for a kinase-dead EGFR variant (D813N) are shown. (B)

Phosphorylation of ERK. The levels of phosphorylated ERK (pERK) show a bimodal distribution, with cells tending to have either low or high levels of pERK. The data are best represented as a histogram of cell numbers with different levels of pERK, as described (Kovacs et al., 2015b). Note that the response of two Domain IV mutants (II/KK and VEN/ERR) resembles that of the wild-type EGFR. For comparison, data for kinase-dead EGFR (D813N) show a reduced population of cells with high levels of pERK. (Adapted from eLife 2016;5:e14107)

5.3 Proximal and distal sites in EGFR tail are phosphorylated differently within a EGFR dimer

To understand why mutations that reduce multimerization affect phosphorylation of the EGFR tail, I carried out co-transfection experiments using EGFR variants that are activator-impaired (i.e., a mutation prevents their kinase domains from taking the activator position in an asymmetric dimer) or receiver-impaired (a mutation prevents their kinase domains from taking the receiver position, but they can serve as activators; see Figure 17A for a schematic representation of these mutants). We showed previously that for such combinations the activator tail is phosphorylated slightly more efficiently than the receiver tail, but we could not distinguish between distal and proximal sites (Kovacs et al., 2015b).

I co-transfected cells with combinations of receiver-impaired and activator-impaired variants of EGFR in which the full-length tail is present on both kinases, but within which specific tyrosine residues are mutated in one tail but not the other. Phosphorylation of Tyr 1173 clearly occurs in both receiver and activator tails, with higher efficiency for the activator tail (Figure 17A), which is consistent with our previous study. For Tyr 992, in the proximal part of the tail, the phosphorylation level in the activator tail is much lower compared to that in the receiver tail (Figure 17B). Tyr 992, in the proximal part of the tail, can only access its own kinase domain in an asymmetric dimer (Koland, 2014). In a combination of receiver-impaired and activator-impaired EGFR molecules, the activator kinase domain is not itself activated, and so Tyr 992 in the activator tail cannot be phosphorylated efficiently. These results suggest that if phosphorylation occurred only within a dimer, then only half the proximal sites would be phosphorylated efficiently, unless the receiver and activator kinases swapped positions.



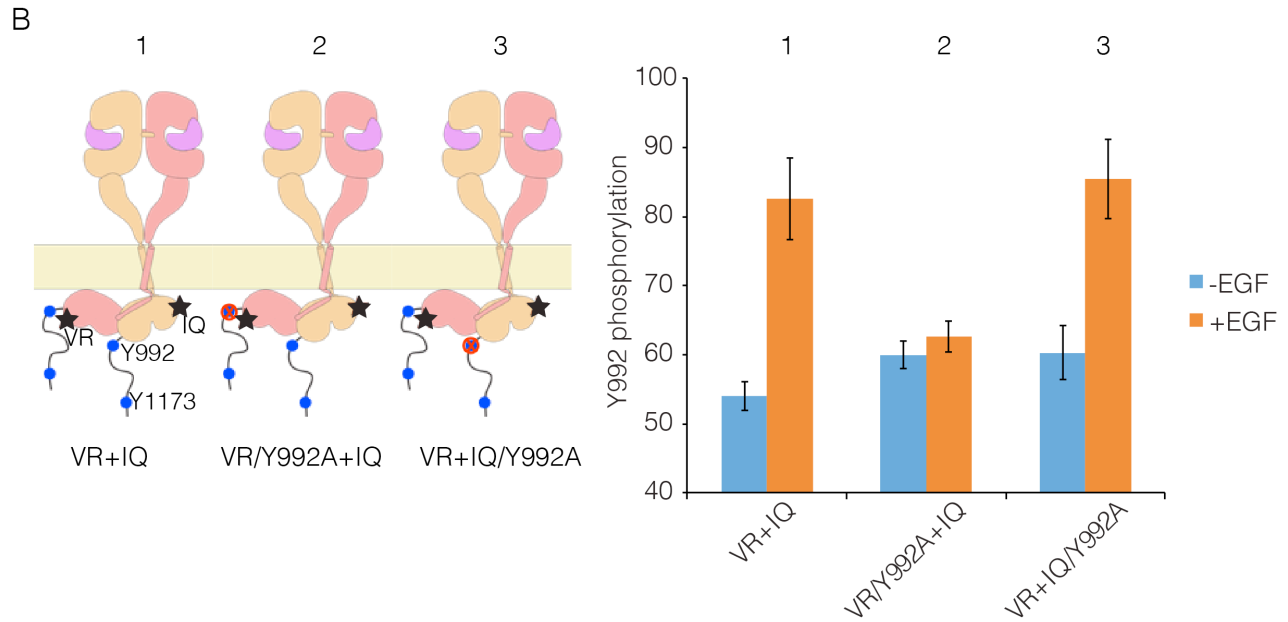


Figure 17 Proximal and distal tail phosphorylation of EGFR in co-transfections with activator-impaired and receiver-impaired mutants.

In these experiments, activator-impaired EGFR (V924R; denoted VR; salmon subunit) is fused to EGFP at the C-terminus and receiver-impaired EGFR (I682Q; denoted IQ; yellow subunit) is fused to mCherry. Phosphorylation is measured after co-transfection of both constructs, with and without EGF. (A) Tyr 1173, located in the distal portion of the tail, is present in both tails (denoted 1), in only the tail of receiver-impaired EGFR (denoted 2) or in only the activator-impaired tail (denoted 3). The bar graphs show phosphorylation levels for Tyr 1173. (B) As in Panel A, for a site in the proximal part of the tail, Tyr 992. Note that addition of EGF leads to only a very small increase in phosphorylation of Tyr 992 when the kinase bearing that residue is receiver-impaired. (Adapted from eLife 2016;5:e14107)

5.4 Lateral phosphorylation is inefficient between EGFR dimers

In considering the potential relevance of multimerization for EGFR activity, I also wondered about the extent to which activated EGFR molecules (“enzymes”) could phosphorylate other EGFR molecules (“bystander substrates”) through random encounters, without the necessity for formation of a specific organization. It has been shown previously, using co-transfection of wild-type and chimeric variants of EGFR, that the phosphorylation of bystander EGFR kinase domains does not occur efficiently (Muthuswamy et al., 1999). I addressed this issue by co-transfecting active EGFR variants lacking Tyr 1173 in the tail (“Enzyme-EGFR”) with EGFR variants that are kinase-dead, but contain Tyr 1173 (“Substrate-EGFR”; see Figure 18).

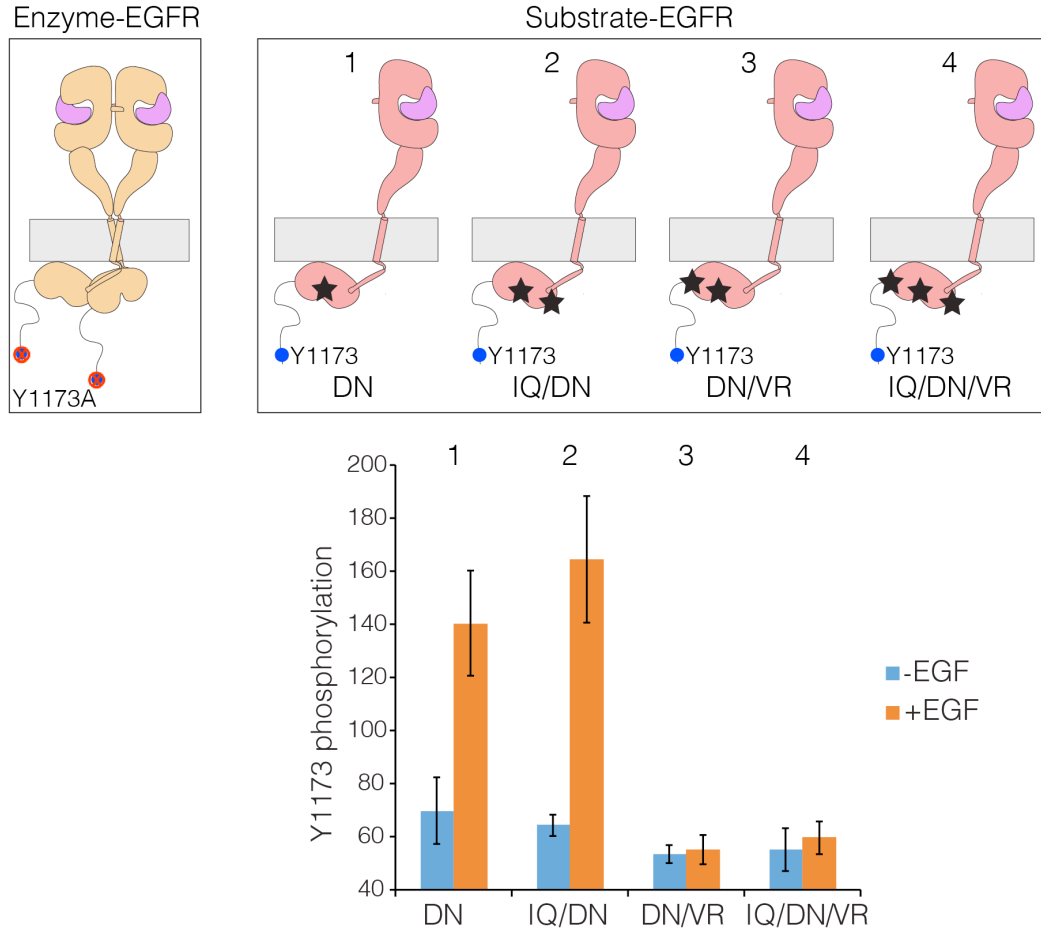


Figure 18 Lateral phosphorylation of the tail of EGFR.

Top) Schematic of kinase-active EGFR (Enzyme-EGFR) that is co-transfected with a kinase-dead variant (D813N; Substrate-EGFR), as shown in the schematic diagram. Tyr 1173 in Enzyme-EGFR is replaced by alanine. Four variants of substrate-EGFR are used: (1) kinase-dead EGFR, with no other mutations, denoted DN, (2) kinase-dead EGFR that is also receiver-impaired, IQ/DN, (3) kinase-dead EGFR that is also activator-impaired, DN/VR, and (4) kinase-dead EGFR that is also activator- and receiver-impaired, IQ/DN/VR. Bottom) Bar graph showing phosphorylation levels for Tyr1173, with and without EGF. Note that Substrate-EGFR that is activator-impaired shows no increase in phosphorylation above the basal level upon EGF addition. (Adapted from eLife 2016;5:e14107)

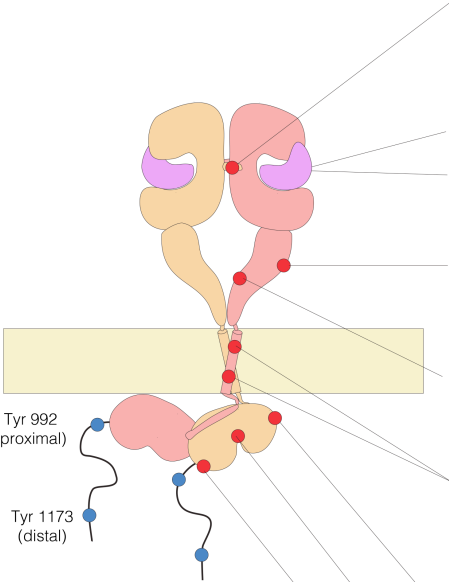
When Enzyme-EGFR is co-transfected with a Substrate-EGFR in which the activator and receiver surfaces are intact, then robust phosphorylation of Tyr 1173 on the Substrate-EGFR is observed (Figure 18). Phosphorylation of Tyr 1173 is also observed when the Substrate-EGFR is receiver-impaired (I682Q) (Figure 18). Strikingly, if the Substrate-EGFR is activator-impaired (V924R), then phosphorylation of Tyr 1173 is not efficient (Figure 18). Likewise, phosphorylation of Tyr 1173 is also not efficient if the substrate-EGFR is both activator-impaired and receiver-impaired (Figure 18). Although a previous study had inferred that lateral phosphorylation of EGFR tails is possible (Ruan and Kannan, 2015), my results lead me to conclude that lateral phosphorylation of the tail in bystander substrates is inefficient, and that for

efficient tail phosphorylation to occur, the kinase bearing the tail has to be part of an asymmetric dimer.

These results suggest that multimerization involving chains of asymmetric dimers of kinase domains might be a mechanism for boosting the phosphorylation of both proximal and distal sites on the tail. In such a multimer model, where the majority of kinase domains are sandwiched by other kinase domains, they function as “activators” and “receivers” simultaneously. Therefore, phosphorylation of the EGFR tail would be potentiated and more easily propagated in response to EGF.

5.5 A model for multimerization in the activation of EGFR

In collaboration with Deepti Karandur, a postdoc in our group, we have constructed a plausible model for an EGFR multimer that is consistent with the constraints implied by our findings (a summary of the key results that we used in constructing this model is provided in Figure 19). Deepti Karandur is the primary developer of this model. The components of the model are the known dimeric arrangements of the extracellular module, the transmembrane helices and the kinase domains, which are connected together to produce a model for dimeric full-length EGFR, as described (Arkhipov et al., 2013a; Endres et al., 2013). We then modeled tetramers of EGFR by packing the dimers against each other as rigid bodies. This model is simply a useful construct for considering how tetramerization might occur, and is not based on detailed energy calculations. Also, the limited set of mutations we have made does not allow us to conclude definitively that the residues that we have identified as being important are responsible for a direct and stereospecific interaction between dimers. Thus, the models should be considered as structural hypotheses that await more rigorous experimental tests.



Mutation or Variation	Effect on Activity	Effect on Multimerization
deletion of dimerization arm: Δ -arm	strong reduction of autophosphorylation in Tyr 992 and Tyr 1173	increases EGF-independent dimerization but has little effect on EGF-induced multimerization modest effect on EGF-induced dimerization
replacement of EGF by TGF- α		no reduction in EGF-induced multimerization
EGF concentration increased from 15 nM to 2 μ M		no reduction in EGF-induced multimerization
mutations in the proposed Domain IV multimerization interface: IIIV/KKRE VEN/ERR TN/RR	reduction in Tyr 992 and Tyr 1173 phosphorylation strong reduction of PI3K phosphorylation no effect on ERK phosphorylation	decreases EGF-dependent multimerization no reduction in EGF-induced dimerization
mutation of the autoinhibitory tether on Domain IV: Δ -tether		increases EGF-independent dimerization
mutations in the transmembrane helix (small residues in the N- and C-terminal interfaces replaced by isoleucine)	modest effect on Tyr 1173 stronger effect on Tyr 992 strong reduction of PI3K phosphorylation no effect on ERK phosphorylation	strong reduction of EGF-dependent multimerization no reduction in EGF-induced dimerization
receiver-impaired (I682Q)	tail can only be phosphorylated within an asymmetric dimer	reduces EGF-dependent multimerization and EGF-independent dimerization when combined with V924R
kinase-dead (D813N)	tail can be phosphorylated only within an asymmetric dimer	no effect on EGF-dependent multimerization
activator-impaired (V924R)		reduces EGF-dependent multimerization and EGF-independent dimerization when combined with I682Q

Figure 19 Summary of EGFR variants studied in this work and their effects on EGFR activity and multimerization.

EGFR autophosphorylation in Tyr 992 and Tyr 1173, and the phosphorylation of PI3K and ERK were monitored by FACS assay using mammalian cells. To analyze the EGFR stoichiometry, with or without EGF, stepwise photobleaching counting experiments were done in *Xenopus* oocytes and PIE-FCCS data was measured in mammalian cells. (Adapted from eLife 2016;5:e14107)

We began by docking two dimers of the extracellular module to generate a tetramer. There are, at present, only two crystal structures for intact extracellular modules of EGFR-family members bound to ligands, EGFR bound to EGF (PDB code: 3NJP; (Lu et al., 2010)), and HER4 bound to neuregulin-1 β (PDB code: 3U7U; (Liu et al., 2012)). The principal difference between these is that the EGFR extracellular module is closed, with the C-terminal tips of the extracellular module are close together, whereas in HER4 they are separated. These differences reflect an intrinsic flexibility in the extracellular module, rather than fundamental difference between EGFR and HER4, as shown by molecular dynamics simulations of EGFR (Arkhipov et al., 2013a). We found that a closed structure, with the tips of Domain IV close together, is more suitable for the generation of multimers in which each subunit retains connection to a planar membrane (see Figure 20).

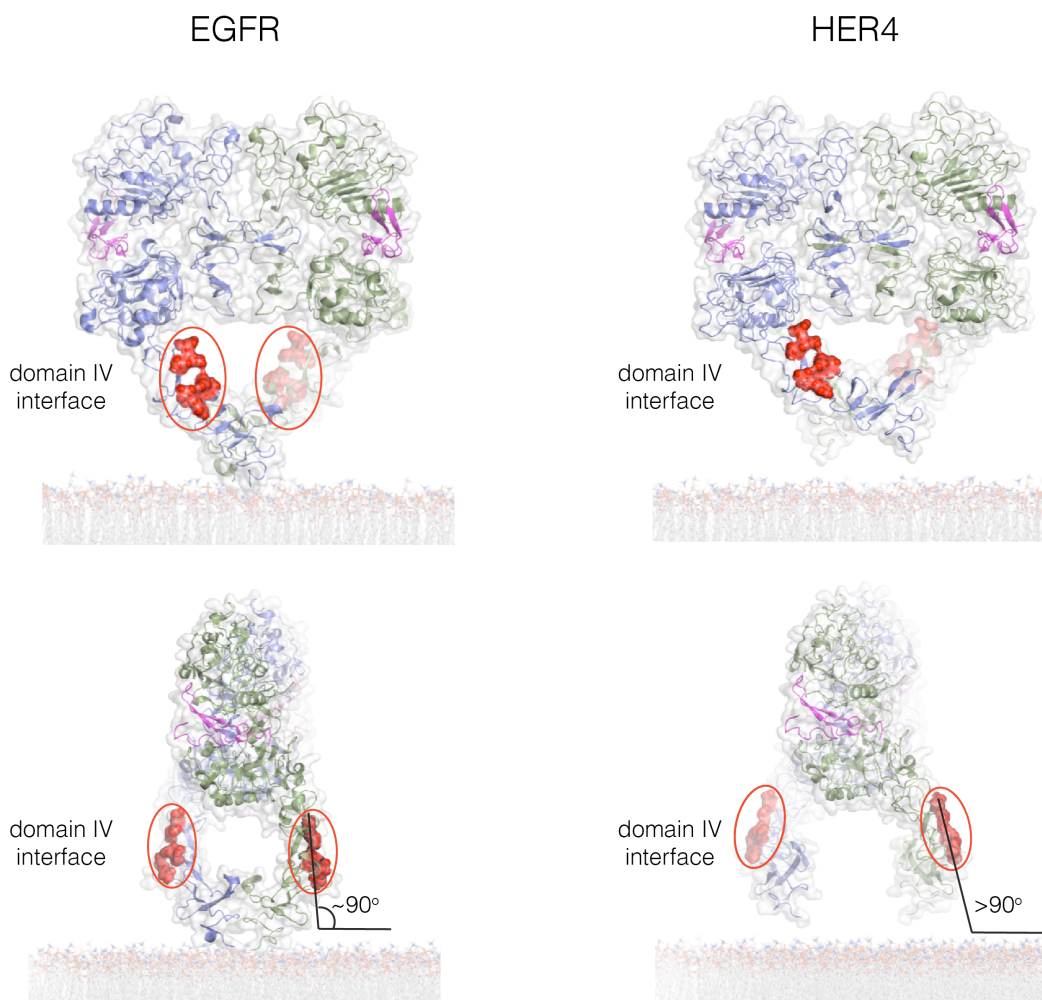


Figure 20 The Domain IV interface in crystal structures of the extracellular dimers of EGFR (left; PDB code 3NJP) and HER4 (right; PDB code 3U7U).

Two orthogonal views of each structure are shown. The C-terminal tips of the extracellular module are close together in EGFR, and further apart in HER4. When the extracellular module is aligned symmetrically with respect to the membrane plane, the configuration of Domain IV in EGFR has the Domain IV multimer interface nearly vertical to the membrane plane. This allows stacking interactions between dimers to be perpetuated while retaining connection to a planar membrane. If the tips are splayed apart, as in the HER4 structure, then stacking between dimers would generate a rotation away from the membrane. For this reason, we used the structure of EGFR to generate a model for the tetramer. (Adapted from eLife 2016;5:e14107)

Using the EGFR dimer (PDB code: 3NJP), we ran ClusPro to generate tetramers, with the constraint that the seven residues in Domain IV that are important for multimerization are at the interface between dimers. This resulted in the generation of a family of tetrameric arrangements of the extracellular module that resemble each other in general (see Figure 21A for a representative model for an extracellular tetramer). The ligand-bound heads of the receptors (Domains I to III) are stacked in a parallel arrangement, with a Domain IV leg from one dimer interacting with a Domain IV leg from the other. These dimers are open structures, and higher-order multimers can be formed readily by adding additional dimers through propagation of the

Domain IV-Domain IV interaction. We checked that the selected ClusPro solutions did not place any of the documented glycosylation sites at the interface between dimers (Zhen et al., 2003).

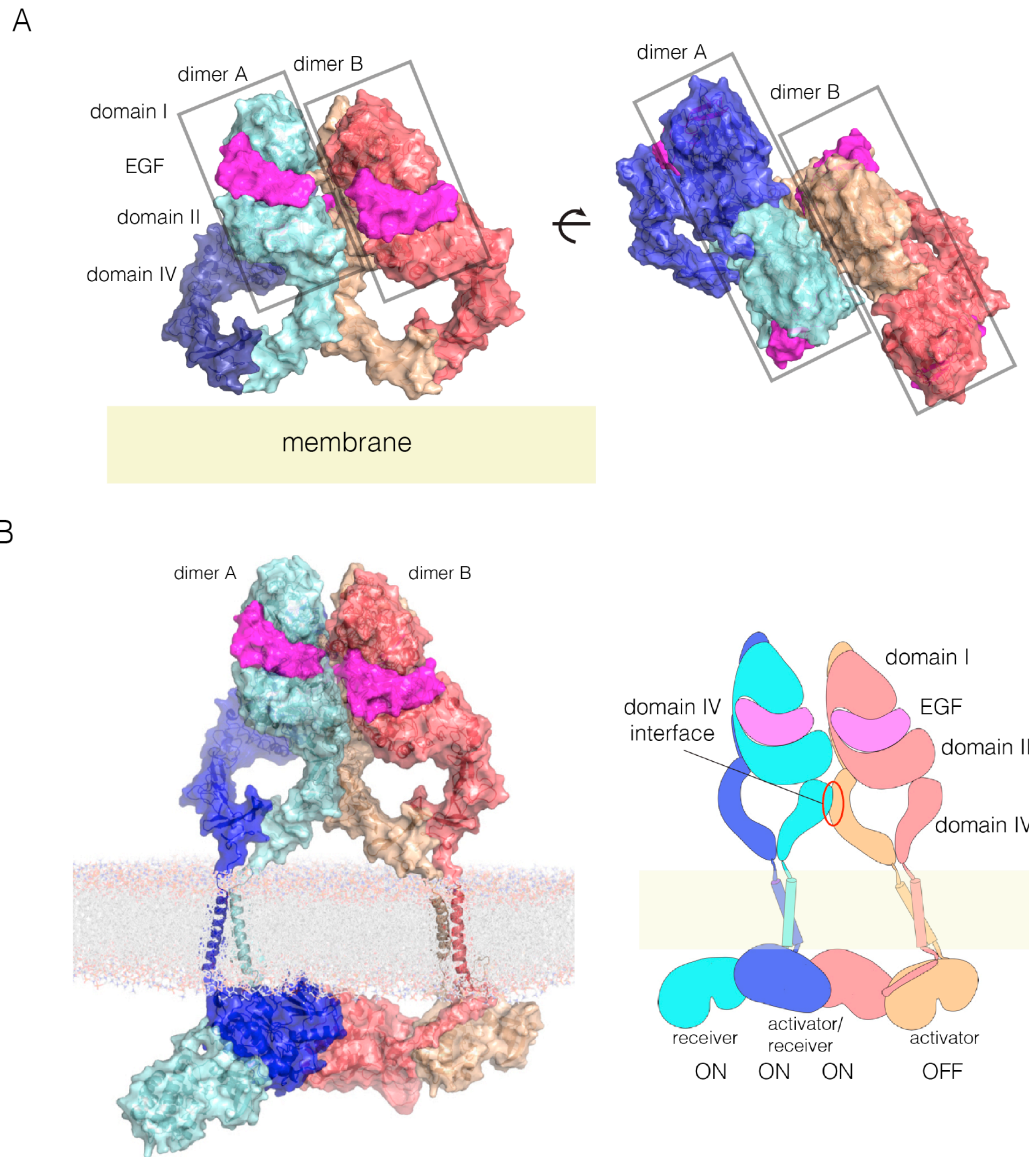


Figure 21 A model for EGFR multimerization.

(A) Two orthogonal views of a tetramer of extracellular modules, selected manually from ClusPro docking dimers (PDB code: 3NJP) with the constraint that the residues in Domain IV that affect multimerization are located at the interface. (B) A model for an EGFR tetramer, generated by connecting the model shown in Panel A to the structure of the dimeric transmembrane helices (PDB code 2M20) and a chain of kinase domains (PDB codes: 2GS6 and 3GOP). A schematic representation of the tetramer is shown on the right. (C) Schematic diagram indicating how higher-order multimers might be generated by repeating the interactions used to generate the model for the tetramer. (Adapted from eLife 2016;5:e14107)

We used the NMR structure of a dimer of the transmembrane helices and the juxtamembrane-A segment embedded in a lipid bilayer to extend the tetramer model (PDB code: 2M20; (Endres et al., 2013)). We connected the N-terminal ends of the transmembrane helices to

the C-terminal ends of each Domain IV. Crystal structures of the kinase domains of EGFR have chains in which each kinase domain can serve as the allosteric activator for the next kinase domain, and can be activated by the previous one (Stamos et al., 2002; Zhang et al., 2006). We generated a chain of four kinase domains based on crystal structures of the EGFR kinase domain (PDB codes: 2GS6 and 3GOP). The first two kinase domains in this model are connected by the juxtamembrane-B latch, which is linked to the dimer of the transmembrane-juxtamembrane-A segments (Arkhipov et al., 2013a). The second two kinase domains are connected similarly. The two pairs are joined by the N-lobe/C-lobe interface that defines the asymmetric dimer, without the juxtamembrane latch. The first three kinase domains in the kinase domains are assumed to be active, while the fourth one is not.

A model for an EGFR tetramer in which all of the components are connected as described is shown in Figure 21B. All-atom molecular dynamics simulations using this model is extremely demanding of computer time. Instead, we generated a coarse-grained representation of the tetramer in a lipid bilayer using the MARTINI force field (Marrink et al., 2007). A 1 microsecond molecular dynamics trajectory using the coarse-grained model indicates that the inter-domain connections and inter-subunit interfaces in the model are plausible, since the tetramer remains intact over this timescale (Figure 22 and Figure 23).

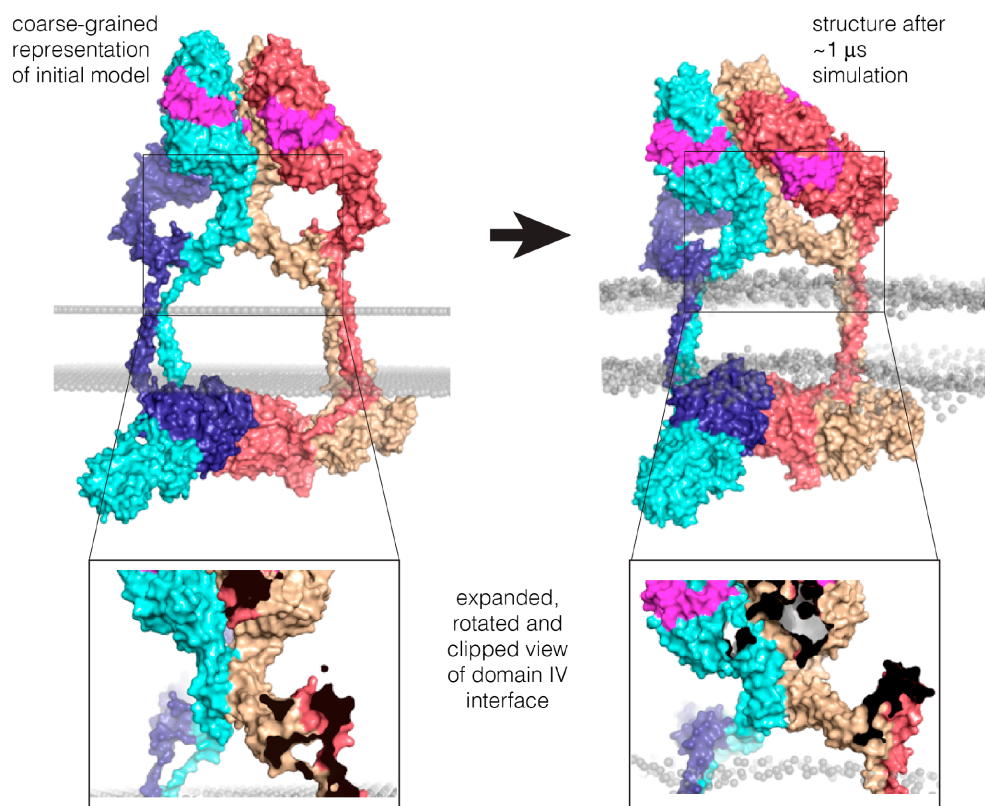


Figure 22 Coarse-grained molecular dynamics simulation in a lipid bilayer.

The model shown in Figure 21B was converted to a coarse-grained representation (Marrink et al., 2007) and inserted in an lipid bilayer, as shown on the left. A 1 μ s molecular dynamics trajectory was generated, and a representative structure towards the end of the trajectory is shown on the right. The Domain IV interface and the interfaces between kinase domains remain stable during the trajectory (see Figure 23). (Adapted from eLife 2016;5:e14107)

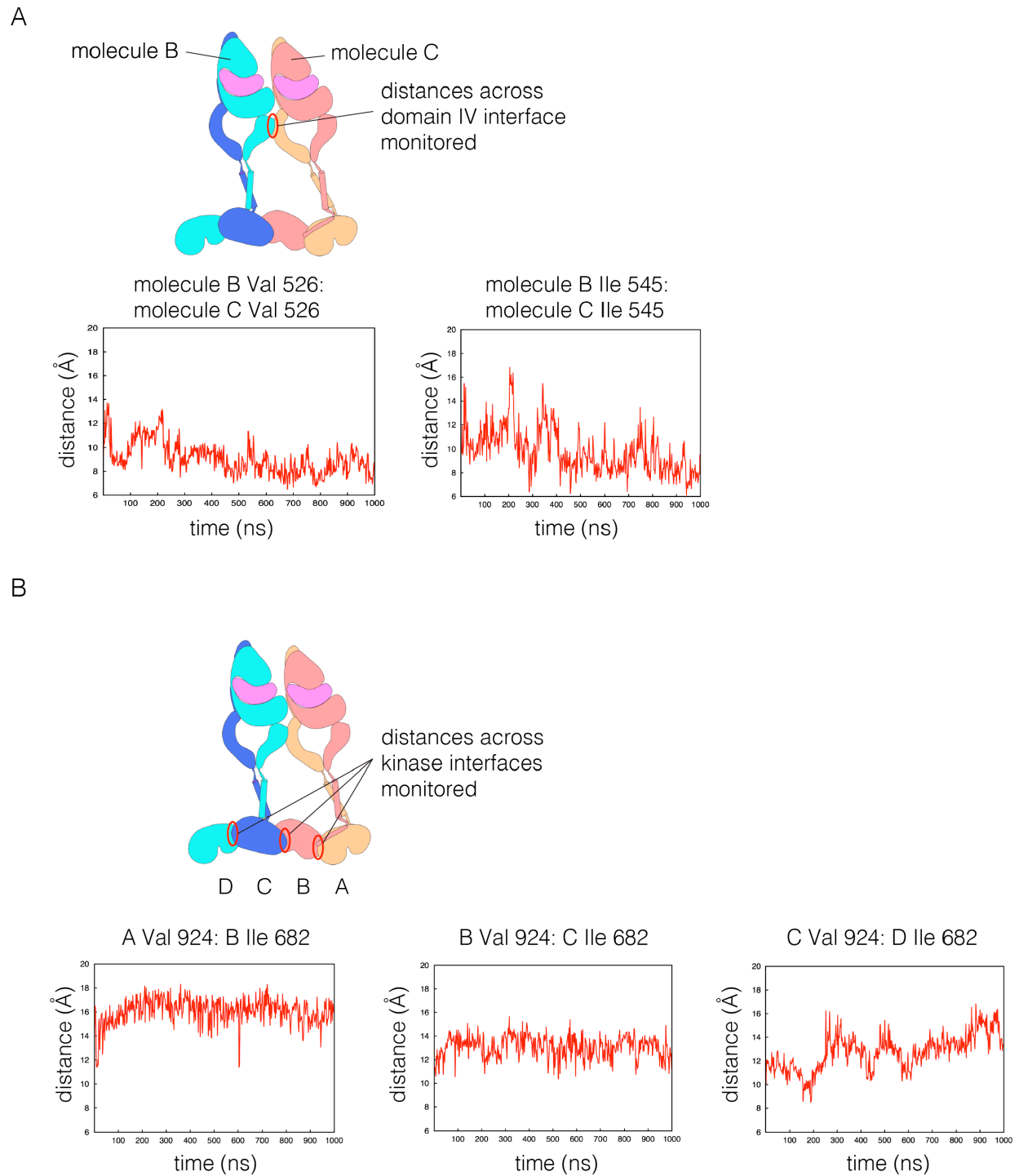


Figure 23 Structural integrity of the tetramer model in coarse-grained molecular dynamics simulation.

(A) The distance between two pairs of residues across the Domain IV simulation are shown over the length of the trajectory. (B) The distance between two residues that are across from each other at each of the three kinase dimer interfaces is shown over the length of the trajectory. For this analysis, the kinases are denoted A, B, C and D, as shown in the schematic diagram. A and B are linked by a juxtamembrane latch, as are C and D. No juxtamembrane latch was included between kinases B and C. The displacement between kinases C and D is larger, as a consequence, but all three interfaces are stable. (Adapted from eLife 2016;5:e14107)

This model can be extended to build a trimer of EGFR dimers, by repeating the interactions from dimer to dimer, as indicated schematically in Figure 24, but the connection between the kinase domains and the transmembrane helices raises a complication. In structures of active EGFR (e.g., PDB Code 2GS6), the rotation between subsequent kinase domains in a chain is 120° . If this rotation is preserved, then the juxtamembrane dimer has to be broken in the third dimer in order to connect to the transmembrane helices. We note that there are structures of the EGFR, HER2 and HER4 kinase domains in inactive conformations in which chains of asymmetric dimers are formed (Aertgeerts et al., 2011; Qiu et al., 2008; Red Brewer et al., 2009). In these chains, the rotation between adjacent kinase domains is 90° , rather than 120° , due to rotation of the N-lobe of the kinase domain with respect to the C-lobe. This intrinsic flexibility in the kinase domain may allow maintenance of the juxtamembrane interactions along the chain, but we have not investigated this further.

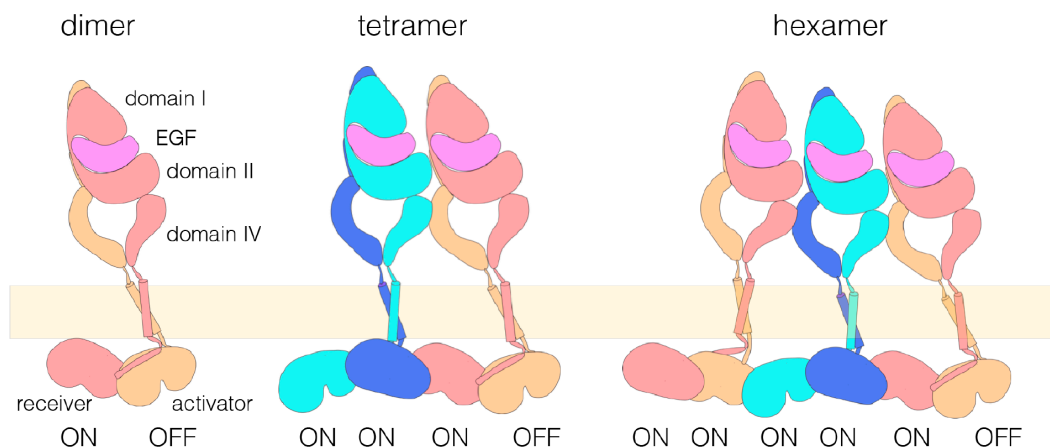


Figure 24 A model for extended EGFR multimerization.

Schematic diagram indicating how higher-order multimers might be generated by repeating the interactions used to generate the model for the tetramer. (Adapted from eLife 2016;5:e14107)

Our model for extended multimers relies on the C-terminal tips of the extracellular module being close together (see Figure 20). A closed conformation of the extracellular module would be stabilized by the dimerization of the transmembrane helices, which brings the N-terminal ends of the helices close together (Endres et al., 2013; Mineev et al., 2010). Such coupling may explain the critical importance of the transmembrane dimer for multimerization. In the *Xenopus* oocyte assay, we found that disruption of the transmembrane dimer interface resulted in a substantial reduction in the extent of multimerization (Figure 10B). In contrast, the deletion of the dimerization arm in the extracellular module (Δ -arm) had very little effect. In terms of its effect on activity, EGFR that is mutated in the transmembrane helix behaves similarly to EGFR with Domain IV mutations that block multimerization, with strong inhibition of PI3K phosphorylation, and only a mild effect on ERK phosphorylation (Figure 25). Deletion of the dimerization arm compromises EGFR function in a more general way, blocking both PI3K and ERK phosphorylation. This differential effect of mutations in the transmembrane helices on proximal versus distal sites may explain why it has been difficult to observe strong effects on EGFR activity by disrupting transmembrane dimerization (Endres et al., 2013; Lu et al., 2010).

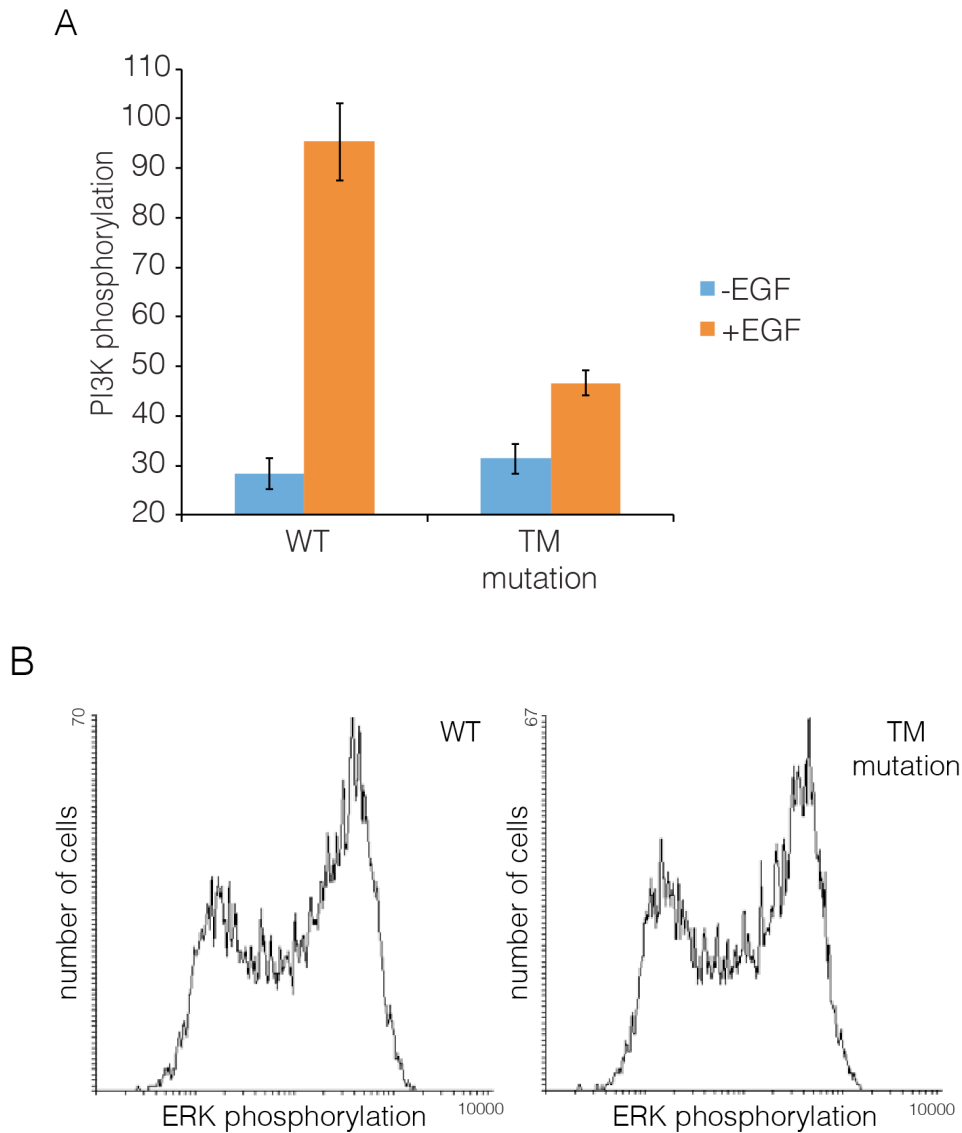


Figure 25 Effects of transmembrane helix mutations on phosphorylation of effector proteins.

(A) PI3K and (B) ERK phosphorylation was measured in cells expressing mutant EGFR, harboring mutations in the transmembrane helix (Thr 624, Gly 625, Gly 628, Gly 629, Ala 637 and Gly 641 are all replaced by isoleucine; compare with Figure 10). Data for PI3K and for ERK are shown as in Figure 16. (Adapted from eLife 2016;5:e14107)

It is possible that this model for multimerization may apply to other human EGFR family members as well. Examination of the Domain IV multimerization interface shows that although there are changes in the identity of residues within this region, the general hydrophobicity of residues in this surface region is conserved. For heterodimers of HER2 and HER3, an interesting possibility is that a tetramer could have two HER2 kinase domains sandwiched between HER3 kinase domains. The HER2 tail is similar in sequence to that of EGFR, and is likely to be subject to the same constraints on the phosphorylation of proximal sites. The HER3 tail is distinctive, and includes a ~70 residue long spacer between the kinase domain and the first phosphorylation site, making HER3 less dependent on a specific organization of kinase domains for

phosphorylation. The first HER2 kinase domain would be activated by HER3, and would serve as the activator for the second HER2 kinase domain. Multimerization has been shown to be important for the phosphorylation of HER2 in HER2-HER3 heterodimers (Zhang et al., 2012), and the simultaneous activation of two HER2 kinase domains in a tetramer might account for this.

Summary

Using mutations identified in Domain IV that specifically affect EGFR multimerization rather than dimerization, I have uncovered a functional role of multimerization in EGFR activation. My analysis of EGFR autophosphorylation and the activation of two downstream signaling pathways has revealed that EGFR multimerization is necessary for robust phosphorylation of PI3K, which is recruited to a tyrosine residue that is located in the proximal part of the tail. I show that if the kinase domains are restricted to only form dimers, the proximal sites on the activator tail are poorly phosphorylated. I also show that lateral phosphorylation of unactivated EGFR by activated EGFR does not happen efficiently outside of asymmetric dimers. These results point to the importance of a higher-order organization of asymmetric dimers for robust EGFR autophosphorylation. We propose a structural model for EGFR multimer that is based on self-association of EGFR dimers and is consistent with our experimental observations described in Chapter 2, 4 and 5.

Concluding Remarks

In this dissertation, I have described my studies on the oligomerization states of EGFR before and after activation, by using a single-molecule based *Xenopus* oocyte assay that I developed together with Shashank Bharill, a postdoc in Ehud Isacoff's group.

We show that the receptor is predominantly monomeric in the absence of EGF, at low expression levels. This is consistent with the canonical model of EGFR activation, in which ligand-free EGFR is monomeric and inactive. However, in our experiments, we did observe a small population of ligand-independent dimers of EGFR, whose existence and function have been widely debated. We tested various EGFR mutants to monitor the nature of this ligand-independent dimer of EGFR, which is of great interest because overexpression of EGFR and other family members results in constitutive activation of the receptor. Our data are consistent with the accepted view, which is that the autoinhibited conformation of the extracellular domain provides a steric block to dimerization. Mutations that disrupt the autoinhibitory conformation of EGFR extracellular domain, can promote the formation of the ligand-independent EGFR dimers. On the intracellular side, EGFR activation involves the allosteric activation of a "receiver" kinase domain in a dimer by the other, the "activator", through the formation of an asymmetric dimer of kinase domains. Mutations that disrupt the asymmetric kinase dimer, can inhibit the formation of the ligand-independent EGFR dimers. Our results emphasize the importance of asymmetric dimer formation by the kinase domains in driving EGFR dimerization, even without the addition of EGF. We speculate that in the absence of EGF, the autoinhibited extracellular domain of EGFR is preventing the receptor from dimerizing, although the kinase domains of EGFR have the tendency to form the asymmetric dimer. In the case of EGFR overexpression, high local density of the receptor could bring the EGFR kinase domains into close proximity and enhance the apparent avidity among kinase domains to form asymmetric dimers. Collectively, these kinase domains could potentially overcome the steric blockage provided by the autoinhibited extracellular domain and become constitutive dimers. These ideas serve as background for the more important discussion that follows.

In the presence of EGF, the steric block in the EGFR extracellular domain is released and the extracellular domains are dimerized. The dimerization of the extracellular domains facilitates the formation of asymmetric kinase domain dimers. More importantly, we found that ligand-induced receptor self-association does not end at dimerization, but continues with the generation of multimers. While the existence of higher-order ligand-induced multimers of EGFR has been reported before (Clayton et al., 2005, 2008), it is very challenging to study the nature and function of these assemblies without a putative model for how they might interact with each other. Our identification of a cluster of residues in Domain IV that specifically affect multimerization rather than dimerization has allowed us to uncover a functional role of multimerization in EGFR activation.

I present a mammalian cell-based analysis of EGFR autophosphorylation and the activation of two downstream signaling pathways. The long C-terminal tail of EGFR has two kinds of phosphorylation sites. Those that are distal to the kinase domain (e.g., Tyr 1068, and Tyr 1173, which recruit the adaptor proteins GRB2 and SHC) are phosphorylated more efficiently than those in the proximal part of the tail (e.g., Tyr 992) (Koland, 2014; Kovacs et al., 2015b). I now show that multimerization is necessary for robust phosphorylation of PI3K, which is recruited to the proximal part of the tail. I also show that if the kinase domains are restricted by mutation to only form dimers, the proximal sites on the activator tail are poorly phosphorylated.

In addition, I show that lateral phosphorylation of unactivated EGFR by activated EGFR does not happen efficiently outside of asymmetric dimers, pointing to the importance of a higher-order organization of asymmetric dimers for robust phosphorylation.

Together with Deepti Karandur, a postdoc in Kuriyan lab, we propose a model for an EGFR tetramer that is consistent with our experimental observations and is based on self-association of EGFR dimers. This model is reminiscent of the arrays formed by the sensor of the unfolded protein response, IRE1, in which oligomerization of the peptide-binding module in the endoplasmic reticulum is coupled to the chaining of kinase domains in the cytoplasm (Korennykh et al., 2009). In IRE1, the chaining of kinase domains occurs in a back-to-front manner, whereas in EGFR our model has the kinase domains chained in a head to tail fashion, generating a continuous array of activator and receiver kinase domains. Such an array might boost tail phosphorylation by stabilizing the active conformations of the majority of kinase domains, and also by facilitating the phosphorylation of the proximal segments of the tail *in cis*.

Our understanding of the mechanism for EGFR activation relies heavily on structural information for fragments of the receptor. However, the efficient activation of EGFR and the initiation of signaling pathways on the cell membrane involves dynamic interactions between intact receptors and their surroundings, including membranes, adaptor proteins, effector proteins, and the cytoskeleton. The multimerization of EGFR may be crucial for signaling in this environment, since it increases the effective density of docking sites for downstream adaptor proteins. These adaptors are typically multivalent, and their docking could synergize with EGFR multimerization, leading to larger-scale clusters. The formation of such signaling platforms may be a central aspect of maintaining the balance between ligand-induced activation and inactivation by receptor internalization, phosphatases or ubiquitin ligases, and will continue to serve as a focus of intense study. We believe that our stoichiometric and functional analysis of EGFR provides a valuable framework for future studies on the structural details and functional consequences of this important family of receptors.

During the course of our investigation into the EGFR stoichiometry in the presence of EGF using *Xenopus* oocytes, we made an unexpected discovery. Upon binding to EGF, EGFR becomes more mobile and starts to move along the microvilli at the oocyte surface. We were initially very surprised by this observation, since it is visually so dramatic to see EGFR traveling in straight lines. Once we learnt that EGFR is moving along the microvilli on the oocyte surface, we were fascinated by the potential of this phenomenon as a functional readout to learn more about EGFR signaling at the single-molecule level in *Xenopus* oocytes. However, before we can go any further and use this as a signaling output of EGFR activation, we need to know the molecular details behind this phenomenon. We tested EGFR mutants and various inhibitors for components that might be involved in this process. Our data suggest that the kinase activity of EGFR is required for this motion to occur, but that the C-terminal tail region is dispensable. While microtubules are not involved, actin cytoskeleton plays critical role in this process. This link between EGFR and actin cytoskeleton turns out to be quite interesting. EGF-stimulated EGFR activation has long been suggested to be actively involved in the reorganization of actin cytoskeleton (Bretscher, 1989; Rijken et al., 1991), primarily through small GTPases Rac and Rho (Peppelenbosch et al., 1993, 1995). But the interplay between EGFR and actin is also found in the other direction, which is that EGFR activation is modulated by its association with the actin cytoskeleton. Although it is still not clear if EGFR could bind to the actin directly *in vivo*, there is overwhelming evidence that actin cytoskeleton plays regulatory role in EGFR activation (van Bergen en Henegouwen et al., 1992; Gronowski and Bertics, 1993, 1995; Hartigh et al.,

1992). After struggling for quite a while, we feel that much more intense studies are required, for uncovering the molecular mechanism of EGF-induced EGFR linear motion on the *Xenopus* oocyte surface.

Materials and Methods

Single-molecule imaging in live *Xenopus* oocytes

For experiments in *Xenopus* oocytes, the human EGFR gene was cloned into pGEMHE-X-EGFP vector at Sall and SacII site to generate a C-terminally EGFP tagged version of EGFR. Messenger RNA (mRNA) was then synthesized in vitro from linearized DNA using mMessage mMachine kit (Ambion). For single molecule imaging by TIRF microscopy, mRNA injection for EGFR-EGFP was optimized for expression. We found that 0.25-0.5ng of mRNA for approximately 20 hours of incubation at 18°C produced uniform diffraction-limited spots when imaged by TIRF microscopy.

In the absence of EGF, imaging of EGFR-EGFP on *Xenopus* oocyte membrane by TIRF microscopy was performed as previously described (Chen et al., 2015; Ulbrich and Isacoff, 2007). Briefly, 10-20 oocytes were manually devitellinized after ~20 hours of expression at 18°C, placed on high refractive index coverslips ($n = 1.78$; Olympus America) and excited using a phoxX 488 (60 mW) laser and, imaged using an Olympus 100 \times , numerical aperture (NA) 1.65 oil immersion objective at room temperature. A 495-nm long-pass dichroic mirror was used at excitation in combination with a 525/50-nm band-pass filter at emission. Five hundred to eight hundred frames at the rate of 20 Hz were acquired using an electron multiplying charge coupled device (EMCCD) camera (Andor iXon DV887).

The *Xenopus* oocytes flatten on the surface of coverslips, and we found that if we added fluorescently labeled EGF to oocytes that had already been placed on the coverslips there was limited access of EGF to the receptors. To overcome this problem we added EGF directly into the imaging buffer first, and then placed the oocytes onto the coverslip of the imaging chamber that contains EGF buffer. The EGF that is used in all other experiments is unlabeled. We noticed that upon addition of EGF the spots corresponding to the receptor were no longer fixed in space but were mobile, which complicates the analysis of photobleaching. We found that the addition of a FLAG-tag to the EGFR at the N-terminus resulted in minimization of motion of the receptor, presumably due to better adherence to the glass. We verified that the inclusion of the FLAG tag did not affect the activity of the receptor as assessed by autophosphorylation in response to EGF in mammalian cells (COS-7) (data not shown).

To observe the effect of EGF on EGFR stoichiometry, we placed the oocytes expressing EGFR-EGFP one by one directly in the chamber containing 15 nM EGF solution in ND96 buffer (5 mM HEPES/NaOH, 96 mM NaCl, 2 mM KCl, 1 mM MgCl₂, 1.8 mM CaCl₂, pH 7.6) placed on the TIRF microscope. Imaging was started almost immediately, with a maximum delay of 1-2 minutes, using the same protocol described above.

Only single, immobile, and diffraction-limited spots were analyzed. The number of bleaching steps was determined manually for each single spot included in the analysis; 1000–2000 spots from 5 to 10 oocytes from three to five different batches were analyzed for most of the constructs.

Analysis of EGFR phosphorylation by flow cytometry

Human EGFR (UniProt accession no. P00533) constructs were cloned into vectors based on the pEGFP-N1 plasmid (Clontech) using XhoI and SacII restriction sites. In co-transfection experiments, EGFP was replaced by monomeric variants of mCherry (Clontech) using BamHI and NotI sites. Cos-7 or HEK-293T cells grown on 6-well plates were transfected with FuGENE (Promega) and serum starved for 12 h. These two cell lines were chosen because of their low

levels of expression of endogenous EGFR and high transfection efficiency. Cells were dissociated by enzyme-free cell dissociation buffer (Gibco), transferred to 96-well plates, and spun down at 1,800 rpm for 3 min. Samples were treated with 100 ng/ml EGF (Sigma-Aldrich) for 2 min at room temperature. After stimulation, cells were immediately fixed in 2% formaldehyde for 10 min. Samples were spun down and permeabilized in ice-cold methanol for 30 min on ice. After rehydration in staining buffer (phosphate-buffered saline (PBS), supplemented with 0.2% bovine serum albumin (BSA) and 1 mM EDTA), cells were stained with 1:100 dilution of primary antibody. Anti-EGFR-pY992 (antibody to phosphorylated EGFR [phosphorylated tyrosine at position 992]) (catalog no. 44-786G) was purchased from ThermoFisher Scientific. Anti-PI3Kinase-p85 (pTyr458)/p55 (Tyr199) (catalog no. 4228) and anti-pErk1/2-pT202/pY204 (catalog no. 4370) antibodies were purchased from Cell Signaling Technology. Anti-EGFR pY1173 (catalog no. sc-12351) was purchased from Santa Cruz Biotechnology. Samples were then stained with 1:100 dilution of anti-rabbit Alexa647-labeled secondary antibody (ThermoFisher Scientific, catalog no. A-21245).

Flow cytometry analysis was done using a BD Bioscience LSR Fortessa cell analyzer (San Jose, CA). EGFP was excited by a 50mW, 488nm, Coherent Sapphire laser, and emission was detected using a 525/50-nm band-pass filter. A 50mW, 561nm, Coherent Sapphire laser was used to excite mCherry, and fluorescence was detected using a 610/20-nm band-pass filter. Alexa647 was excited by a 50mW, 640nm laser.

In experiments where only one type of receptor was transfected, cells were binned based on their EGFR-EGFP expression levels, and the mean and standard error values were calculated for the antibody-labeling channel (Alexa647) to obtain a receptor expression dependent phosphorylation plots. In co-transfection experiments, cells were gated first by their expression levels of the two cotransfected constructs, one labeled with mCherry and the other with EGFP. Only cells that are simultaneously expressing comparable levels of mCherry and EGFP, which are majority of the cells, are binned based on their expression levels of the EGFR-EGFP. Mean and standard error values for the Alexa647 fluorescence intensities, corresponding to phosphorylation levels, were calculated in each bin.

Analysis of EGFR surface expression by fluorescence microscopy

Human EGFR was modified with an N-terminal 3 x HA tag (after the signal sequence) and a C-terminal Venus fluorescent protein. HEK-293T cells were transfected with this construct by CaPO₄ and plated at 75% confluency on Poly-D-lysine coated 1.5 mm glass bottom 10 cm dishes. 48 hrs after transfection, the cells were starved in staining media (clear MEM supplemented with 10 mM HEPES pH 7.4, 2 mM L-glutamine and 5% BSA) for 1 hr then stained on ice for 45 min with rabbit anti-HA (Cell Signaling, catalog no. 3724) at a 1:1000 dilution in staining media. Cells were then fixed in 4% paraformaldehyde, blocked for 30 min in staining media and secondary antibody staining (Alex-fluor 647 conjugated goat anti-rabbit, ThermoFisher, A-21244) at 1:1000 dilution in staining media. High resolution images were collected on a Nikon TE-2000 inverted microscope with a 100X objective. Venus was pseudocolored cyan and 647 was pseudocolored magenta. Images for quantification were collected with a 20X objective and analyzed automatically using Nikon's NIS-elements software to determine regions of interest (ROI) based on intensity thresholds of the total (Venus) receptor channel. Surface/total ratio of each ROI was averaged for each day and plotted for one representative experiment. The same camera and laser settings were used for all images collected.

Docking of EGFR by ClusPro

The crystal structure of the dimer of extracellular domain of EGFR bound to EGF (PDBID 3NJP) was docked against itself using ClusPro (Kozakov et al., 2013). For initial docking, we excluded the Domain IV “leg” so that docking was carried out using just the Domains I, II and III “head” regions. We then used Cluspro to dock the entire extracellular domain against itself, with the added constraint that the residues identified by mutation studies to play a role in oligomerization (Val 526, Glu 527, Asn 528, Ile 545, Thr 548, Asn 554 and Ile 556) are at the interface. We manually filtered the ClusPro solutions using three criteria: (i) the C-terminal ends of both dimers must point towards to same plane, (ii) the rotation between the dimers must be small enough to permit the multimer to be extended while retaining connection to the same plane and (iii) documented sites of glycosylation (Zhen et al., 2003) should not be buried at the interface. Application of these filters yielded a family of 6 models that differed from each other only with respect to the tilt and rotation between two dimeric units. We chose a representative one to construct a model for a tetramer of full-length EGFR.

Molecular dynamics simulation of EGFR Tetramer

A representative model of the tetramer was constructed as described in the main text. Missing residues in the connections between different domains were built using PyMOL (The PyMOL Molecular Graphics System, Version 1.8 Schrödinger, LLC.). The complete tetramer structure was energy-minimized using an all-atom force field in the program AMBER (Case et al., 2005). The model was converted to a coarse-grained representation using the Martinize program (Monticelli et al., 2008) and inserted into a lipid bilayer comprised of Dipalmitoylphosphatidylcholine (DPPC) and solvated using the *insane* program (Wassenaar et al., 2015). The final system comprised 1491 and 1461 DPPC molecules in the lipids in the extracellular-facing and intracellular-facing leaflets of the membrane, respectively. The system had Na⁺ and Cl⁻ ions at 0.15 M. GROMACS (Pronk et al., 2013) was used to generate a molecular dynamics trajectory using the coarse-grained representation and the MARTINI force field (Monticelli et al., 2008). The overall structures of the individual EGFR subunits and EGF was maintained with an elastic network model, with no such constraints applied between different subunits. Harmonic restraints were applied between pairs backbone atoms within a subunit, with a bond cut-off between 5 Å and 9 Å, and a force constant of 5 kJ mol⁻¹Å⁻². The energy of the system was minimized using the steepest descent method, first while holding the protein fixed, and then while allowing all the atoms to move. The lipid bilayer was then allowed to equilibrate while holding the protein fixed for 40 ns. Pressure was held constant at 1 bar using the Berendsen algorithm (Berendsen et al., 1984) with a compressibility of 5.0 x 10⁻⁵ bar⁻¹ and a time constant of 10 ps. Pressure control was applied independently in the plane of the membrane, and normal to it. Temperature was maintained at 323 K by rescaling the velocity of all particles (Bussi et al., 2007) with a time constant of 1 ps. Electrostatic interactions were shifted to zero between 0.0 Å and 12.0 Å. Van der Waals interactions were shifted to zero between 9.0 Å and 12.0 Å. A time step of 20 fs was used. The system was then allowed to run for 1 μs in at constant temperature (T=323 K) and pressure (P=1 bar) using the same parameters as for the equilibration run, with the following differences. Pressure was controlled using Parrinello-Rahman algorithm (Parrinello, 1981). Electrostatic interactions were shifted to zero between 0.0 Å and 11.0 Å. Van der Waals interactions were shifted to zero between 9.0 Å and 11.0 Å.

References

Aertgeerts, K., Skene, R., Yano, J., Sang, B.C., Zou, H., Snell, G., Jennings, A., Iwamoto, K., Habuka, N., Hirokawa, A., et al. (2011). Structural analysis of the mechanism of inhibition and allosteric activation of the kinase domain of HER2 protein. *J Biol Chem* 286, 18756–18765.

Alvarado, D., Klein, D.E., and Lemmon, M.A. (2010). Structural basis for negative cooperativity in growth factor binding to an EGF receptor. *Cell* 142, 568–579.

Arkhipov, A., Shan, Y., Das, R., Endres, N.F., Eastwood, M.P., Wemmer, D.E., Kuriyan, J., and Shaw, D.E. (2013a). Architecture and membrane interactions of the EGF receptor. *Cell* 152, 557–569.

Arkhipov, A., Shan, Y., Kim, E.T., Dror, R.O., and Shaw, D.E. (2013b). Her2 activation mechanism reflects evolutionary preservation of asymmetric ectodomain dimers in the human EGFR family. *Elife* 2, e00708.

Batzer, A.G., Rotin, D., Ureña, J.M., Skolnik, E.Y., and Schlessinger, J. (1994). Hierarchy of binding sites for Grb2 and Shc on the epidermal growth factor receptor. *Mol Cell Biol* 14, 5192–5201.

Berendsen, H., Postma, J., van Gunsteren, W., DiNola, A., and Haak, J. (1984). Molecular dynamics with coupling to an external bath. *J. Chem. Phys.* 81, 3684.

van Bergen en Henegouwen, P.M., Hartigh, J.C. den, Romeyn, P., Verkleij, A.J., and Boonstra, J. (1992). The epidermal growth factor receptor is associated with actin filaments. *Exp Cell Res* 199, 90–97.

Bessman, N.J., Bagchi, A., Ferguson, K.M., and Lemmon, M.A. (2014). Complex relationship between ligand binding and dimerization in the epidermal growth factor receptor.

Cell Rep 9, 1306–1317.

Bretscher, A. (1983). Molecular architecture of the microvillus cytoskeleton. *Ciba Found Symp* 95, 164–179.

Bretscher, A. (1989). Rapid phosphorylation and reorganization of ezrin and spectrin accompany morphological changes induced in A-431 cells by epidermal growth factor. *J Cell Biol* 108, 921–930.

Bussi, G., Donadio, D., and Parrinello, M. (2007). Canonical sampling through velocity rescaling. *J Chem Phys* 126, 014101.

Case, D.A., Cheatham, T.E., Darden, T., Gohlke, H., Luo, R., Merz, K.M., Onufriev, A., Simmerling, C., Wang, B., and Woods, R.J. (2005). The Amber biomolecular simulation programs. *J Comput Chem* 26, 1668–1688.

Chen, Y., Bharill, S., Isacoff, E.Y., and Chalfie, M. (2015). Subunit composition of a DEG/ENaC mechanosensory channel of *Caenorhabditis elegans*. *Proc Natl Acad Sci U S A* 112, 11690–11695.

Chung, I., Akita, R., Vandlen, R., Toomre, D., Schlessinger, J., and Mellman, I. (2010). Spatial control of EGF receptor activation by reversible dimerization on living cells. *Nature* 464, 783–787.

Citri, A., Skaria, K.B., and Yarden, Y. (2003). The deaf and the dumb: the biology of ErbB-2 and ErbB-3. *Exp Cell Res* 284, 54–65.

Clayton, A.H., Walker, F., Orchard, S.G., Henderson, C., Fuchs, D., Rothacker, J., Nice, E.C., and Burgess, A.W. (2005). Ligand-induced dimer-tetramer transition during the activation of the cell surface epidermal growth factor receptor-A multidimensional microscopy analysis. *J Biol Chem* 280, 30392–30399.

Clayton, A.H., Orchard, S.G., Nice, E.C., Posner, R.G., and Burgess, A.W. (2008). Predominance of activated EGFR higher-order oligomers on the cell surface. *Growth Factors* 26, 316–324.

Clayton, A.H.A., Tavarneresi, M.L., and Johns, T.G. (2007). Unligated epidermal growth factor receptor forms higher order oligomers within microclusters on A431 cells that are sensitive to tyrosine kinase inhibitor binding. *Biochemistry* 46, 4589–4597.

Dawson, J.P., Berger, M.B., Lin, C.C., Schlessinger, J., Lemmon, M.A., and Ferguson, K.M. (2005). Epidermal growth factor receptor dimerization and activation require ligand-induced conformational changes in the dimer interface. *Mol Cell Biol* 25, 7734–7742.

Dawson, J.P., Bu, Z., and Lemmon, M.A. (2007). Ligand-induced structural transitions in ErbB receptor extracellular domains. *Structure* 15, 942–954.

Endres, N.F., Das, R., Smith, A.W., Arkhipov, A., Kovacs, E., Huang, Y., Pelton, J.G., Shan, Y., Shaw, D.E., Wemmer, D.E., et al. (2013). Conformational coupling across the plasma membrane in activation of the EGF receptor. *Cell* 152, 543–556.

Endres, N.F., Barros, T., Cantor, A.J., and Kuriyan, J. (2014). Emerging concepts in the regulation of the EGF receptor and other receptor tyrosine kinases. *Trends Biochem Sci* 39, 437–446.

Ferguson, K.M., Berger, M.B., Mendrola, J.M., Cho, H.S., Leahy, D.J., and Lemmon, M.A. (2003). EGF activates its receptor by removing interactions that autoinhibit ectodomain dimerization. *Mol Cell* 11, 507–517.

Fleishman, S.J., Schlessinger, J., and Ben-Tal, N. (2002). A putative molecular-activation switch in the transmembrane domain of erbB2. *Proc Natl Acad Sci U S A* 99, 15937–15940.

Garrett, T.P., McKern, N.M., Lou, M., Elleman, T.C., Adams, T.E., Lovrecz, G.O., Zhu,

H.J., Walker, F., Frenkel, M.J., Hoyne, P.A., et al. (2002). Crystal structure of a truncated epidermal growth factor receptor extracellular domain bound to transforming growth factor alpha. *Cell* *110*, 763–773.

Gong, Y., Renigunta, V., Zhou, Y., Sunq, A., Wang, J., Yang, J., Renigunta, A., Baker, L.A., and Hou, J. (2015). Biochemical and biophysical analyses of tight junction permeability made of claudin-16 and claudin-19 dimerization. *Mol Biol Cell* *26*, 4333–4346.

Gronowski, A.M., and Bertics, P.J. (1993). Evidence for the potentiation of epidermal growth factor receptor tyrosine kinase activity by association with the detergent-insoluble cellular cytoskeleton: analysis of intact and carboxy-terminally truncated receptors. *Endocrinology* *133*, 2838–2846.

Gronowski, A.M., and Bertics, P.J. (1995). Modulation of epidermal growth factor receptor interaction with the detergent-insoluble cytoskeleton and its effects on receptor tyrosine kinase activity. *Endocrinology* *136*, 2198–2205.

Hartigh, J.C. den, van Bergen en Henegouwen, P.M., Verkleij, A.J., and Boonstra, J. (1992). The EGF receptor is an actin-binding protein. *J Cell Biol* *119*, 349–355.

Hasson, T. (2003). Myosin VI: two distinct roles in endocytosis. *J Cell Sci* *116*, 3453–3461.

Heinzmann, U., and Höfler, H. (1994). Detection of epidermal growth factor receptor by scanning electron microscopy. *Histochemistry* *101*, 127–134.

Jain, A., Liu, R., Ramani, B., Arauz, E., Ishitsuka, Y., Ragunathan, K., Park, J., Chen, J., Xiang, Y.K., and Ha, T. (2011). Probing cellular protein complexes using single-molecule pull-down. *Nature* *473*, 484–488.

Jones, J.T., Akita, R.W., and Sliwkowski, M.X. (1999). Binding specificities and

affinities of egf domains for ErbB receptors. *FEBS Lett* 447, 227–231.

Jones, R.B., Gordus, A., Krall, J.A., and MacBeath, G. (2006). A quantitative protein interaction network for the ErbB receptors using protein microarrays. *Nature* 439, 168–174.

Jura, N., Endres, N.F., Engel, K., Deindl, S., Das, R., Lamers, M.H., Wemmer, D.E., Zhang, X., and Kuriyan, J. (2009a). Mechanism for activation of the EGF receptor catalytic domain by the juxtamembrane segment. *Cell* 137, 1293–1307.

Jura, N., Shan, Y., Cao, X., Shaw, D.E., and Kuriyan, J. (2009b). Structural analysis of the catalytically inactive kinase domain of the human EGF receptor 3. *Proc Natl Acad Sci U S A* 106, 21608–21613.

Jura, N., Zhang, X., Endres, N.F., Seeliger, M.A., Schindler, T., and Kuriyan, J. (2011). Catalytic control in the EGF receptor and its connection to general kinase regulatory mechanisms. *Mol Cell* 42, 9–22.

Kapus, A., and Janmey, P. (2013). Plasma membrane--cortical cytoskeleton interactions: a cell biology approach with biophysical considerations. *Compr Physiol* 3, 1231–1281.

Koland, J.G. (2014). Coarse-grained molecular simulation of epidermal growth factor receptor protein tyrosine kinase multi-site self-phosphorylation. *PLoS Comput Biol* 10, e1003435.

Korennykh, A.V., Egea, P.F., Korostelev, A.A., Finer-Moore, J., Zhang, C., Shokat, K.M., Stroud, R.M., and Walter, P. (2009). The unfolded protein response signals through high-order assembly of Ire1. *Nature* 457, 687–693.

Kovacs, E., Zorn, J.A., Huang, Y., Barros, T., and Kuriyan, J. (2015a). A structural perspective on the regulation of the epidermal growth factor receptor. *Annu Rev Biochem* 84, 739–764.

Kovacs, E., Das, R., Wang, Q., Collier, T.S., Cantor, A., Huang, Y., Wong, K., Mirza, A., Barros, T., Grob, P., et al. (2015b). Analysis of the Role of the C-Terminal Tail in the Regulation of the Epidermal Growth Factor Receptor. *Mol Cell Biol* 35, 3083–3102.

Kozakov, D., Beglov, D., Bohnood, T., Mottarella, S.E., Xia, B., Hall, D.R., and Vajda, S. (2013). How good is automated protein docking? *Proteins*.

Kozer, N., Henderson, C., Jackson, J.T., Nice, E.C., Burgess, A.W., and Clayton, A.H.A. (2011). Evidence for extended YFP-EGFR dimers in the absence of ligand on the surface of living cells. *Phys Biol* 8, 066002.

Kozer, N., Barua, D., Orchard, S., Nice, E.C., Burgess, A.W., Hlavacek, W.S., and Clayton, A.H. (2013). Exploring higher-order EGFR oligomerisation and phosphorylation--a combined experimental and theoretical approach. *Mol Biosyst* 9, 1849–1863.

Kozer, N., Barua, D., Henderson, C., Nice, E.C., Burgess, A.W., Hlavacek, W.S., and Clayton, A.H. (2014). Recruitment of the adaptor protein Grb2 to EGFR tetramers. *Biochemistry* 53, 2594–2604.

Kwiatkowska, K., Khrebtukova, I.A., Gudkova, D.A., Pinaev, G.P., and Sobota, A. (1991). Actin-binding proteins involved in the capping of epidermal growth factor receptors in A431 cells. *Exp Cell Res* 196, 255–263.

Leahy, D.J. (2004). Structure and function of the epidermal growth factor (EGF/ErbB) family of receptors. *Adv Protein Chem* 68, 1–27.

Lemmon, M.A., Bu, Z., Ladbury, J.E., Zhou, M., Pinchasi, D., Lax, I., Engelman, D.M., and Schlessinger, J. (1997). Two EGF molecules contribute additively to stabilization of the EGFR dimer. *EMBO J* 16, 281–294.

Lemmon, M.A., Schlessinger, J., and Ferguson, K.M. (2014). The EGFR family: not so

prototypical receptor tyrosine kinases. *Cold Spring Harb Perspect Biol* 6, a020768.

Lidke, D.S., Lidke, K.A., Rieger, B., Jovin, T.M., and Arndt-Jovin, D.J. (2005). Reaching out for signals: filopodia sense EGF and respond by directed retrograde transport of activated receptors. *J Cell Biol* 170, 619–626.

Liu, P., Cleveland, T.E., Bouyain, S., Byrne, P.O., Longo, P.A., and Leahy, D.J. (2012). A single ligand is sufficient to activate EGFR dimers. *Proc Natl Acad Sci U S A* 109, 10861–10866.

Lu, C., Mi, L.Z., Grey, M.J., Zhu, J., Graef, E., Yokoyama, S., and Springer, T.A. (2010). Structural evidence for loose linkage between ligand binding and kinase activation in the epidermal growth factor receptor. *Mol Cell Biol* 30, 5432–5443.

Lynch, T.J., Bell, D.W., Sordella, R., Gurubhagavatula, S., Okimoto, R.A., Brannigan, B.W., Harris, P.L., Haserlat, S.M., Supko, J.G., Haluska, F.G., et al. (2004). Activating mutations in the epidermal growth factor receptor underlying responsiveness of non-small-cell lung cancer to gefitinib. *N Engl J Med* 350, 2129–2139.

Macdonald, J.L., and Pike, L.J. (2008). Heterogeneity in EGF-binding affinities arises from negative cooperativity in an aggregating system. *Proc Natl Acad Sci U S A* 105, 112–117.

Margolis, B.L., Lax, I., Kris, R., Dombalagian, M., Honegger, A.M., Howk, R., Givol, D., Ullrich, A., and Schlessinger, J. (1989). All autophosphorylation sites of epidermal growth factor (EGF) receptor and HER2/neu are located in their carboxyl-terminal tails. Identification of a novel site in EGF receptor. *J Biol Chem* 264, 10667–10671.

Marrink, S.J., Risselada, H.J., Yefimov, S., Tieleman, D.P., and de Vries, A.H. (2007). The MARTINI force field: coarse grained model for biomolecular simulations. *J Phys Chem B* 111, 7812–7824.

Mattila, P.K., and Lappalainen, P. (2008). Filopodia: molecular architecture and cellular functions. *Nat Rev Mol Cell Biol* 9, 446–454.

Mendrola, J.M., Berger, M.B., King, M.C., and Lemmon, M.A. (2002). The single transmembrane domains of ErbB receptors self-associate in cell membranes. *J Biol Chem* 277, 4704–4712.

Mineev, K.S., Bocharov, E.V., Pustovalova, Y.E., Bocharova, O.V., Chupin, V.V., and Arseniev, A.S. (2010). Spatial structure of the transmembrane domain heterodimer of ErbB1 and ErbB2 receptor tyrosine kinases. *J Mol Biol* 400, 231–243.

Monticelli, L., Kandasamy, S.K., Periole, X., Larson, R.G., Tieleman, D.P., and Marrink, S.J. (2008). The MARTINI Coarse-Grained Force Field: Extension to Proteins. *J Chem Theory Comput* 4, 819–834.

Mukherjee, T.M., and Williams, A.W. (1967). A comparative study of the ultrastructure of microvilli in the epithelium of small and large intestine of mice. *J Cell Biol* 34, 447–461.

Müller, B.K., Zaychikov, E., Bräuchle, C., and Lamb, D.C. (2005). Pulsed interleaved excitation. *Biophys J* 89, 3508–3522.

Muthuswamy, S.K., Gilman, M., and Brugge, J.S. (1999). Controlled dimerization of ErbB receptors provides evidence for differential signaling by homo- and heterodimers. *Mol Cell Biol* 19, 6845–6857.

Nagy, P., Claus, J., Jovin, T.M., and Arndt-Jovin, D.J. (2010). Distribution of resting and ligand-bound ErbB1 and ErbB2 receptor tyrosine kinases in living cells using number and brightness analysis. *Proc Natl Acad Sci U S A* 107, 16524–16529.

Ogiso, H., Ishitani, R., Nureki, O., Fukai, S., Yamanaka, M., Kim, J.H., Saito, K., Sakamoto, A., Inoue, M., Shirouzu, M., et al. (2002). Crystal structure of the complex of human

epidermal growth factor and receptor extracellular domains. *Cell* *110*, 775–787.

Opresko, L.K., and Wiley, H.S. (1990). Functional reconstitution of the human epidermal growth factor receptor system in *Xenopus* oocytes. *J Cell Biol* *111*, 1661–1671.

Ozcan, F., Klein, P., Lemmon, M.A., Lax, I., and Schlessinger, J. (2006). On the nature of low- and high-affinity EGF receptors on living cells. *Proc Natl Acad Sci U S A* *103*, 5735–5740.

Paez, J.G., Jänne, P.A., Lee, J.C., Tracy, S., Greulich, H., Gabriel, S., Herman, P., Kaye, F.J., Lindeman, N., Boggon, T.J., et al. (2004). EGFR mutations in lung cancer: correlation with clinical response to gefitinib therapy. *Science* *304*, 1497–1500.

Pao, W., Miller, V., Zakowski, M., Doherty, J., Politi, K., Sarkaria, I., Singh, B., Heelan, R., Rusch, V., Fulton, L., et al. (2004). EGF receptor gene mutations are common in lung cancers from “never smokers” and are associated with sensitivity of tumors to gefitinib and erlotinib. *Proc Natl Acad Sci U S A* *101*, 13306–13311.

Parrinello, M. (1981). Polymorphic transitions in single crystals: A new molecular dynamics method. *J Appl Phys* *52*, 7182.

Peppelenbosch, M.P., Tertoolen, L.G., Hage, W.J., and de Laat, S.W. (1993). Epidermal growth factor-induced actin remodeling is regulated by 5-lipoxygenase and cyclooxygenase products. *Cell* *74*, 565–575.

Peppelenbosch, M.P., Qiu, R.G., de Vries-Smits, A.M., Tertoolen, L.G., de Laat, S.W., McCormick, F., Hall, A., Symons, M.H., and Bos, J.L. (1995). Rac mediates growth factor-induced arachidonic acid release. *Cell* *81*, 849–856.

Pike, L.J. (2012). Negative co-operativity in the EGF receptor. *Biochem Soc Trans* *40*, 15–19.

Pronk, S., Páll, S., Schulz, R., Larsson, P., Bjelkmar, P., Apostolov, R., Shirts, M.R., Smith, J.C., Kasson, P.M., van der Spoel, D., et al. (2013). GROMACS 4.5: a high-throughput and highly parallel open source molecular simulation toolkit. *Bioinformatics* 29, 845–854.

Qiu, C., Tarrant, M.K., Choi, S.H., Sathyamurthy, A., Bose, R., Banjade, S., Pal, A., Bornmann, W.G., Lemmon, M.A., Cole, P.A., et al. (2008). Mechanism of activation and inhibition of the HER4/ErbB4 kinase. *Structure* 16, 460–467.

Red Brewer, M., Choi, S.H., Alvarado, D., Moravcevic, K., Pozzi, A., Lemmon, M.A., and Carpenter, G. (2009). The juxtamembrane region of the EGF receptor functions as an activation domain. *Mol Cell* 34, 641–651.

Red Brewer, M., Yun, C.H., Lai, D., Lemmon, M.A., Eck, M.J., and Pao, W. (2013). Mechanism for activation of mutated epidermal growth factor receptors in lung cancer. *Proc Natl Acad Sci U S A* 110, E3595–E3604.

Rijken, P.J., Hage, W.J., van Bergen en Henegouwen, P.M., Verkleij, A.J., and Boonstra, J. (1991). Epidermal growth factor induces rapid reorganization of the actin microfilament system in human A431 cells. *J Cell Sci* 100 (Pt 3), 491–499.

Ritchie, K., Iino, R., Fujiwara, T., Murase, K., and Kusumi, A. (2003). The fence and picket structure of the plasma membrane of live cells as revealed by single molecule techniques (Review). *Mol Membr Biol* 20, 13–18.

Roberts, R., Lister, I., Schmitz, S., Walker, M., Veigel, C., Trinick, J., Buss, F., and Kendrick-Jones, J. (2004). Myosin VI: cellular functions and motor properties. *Philos Trans R Soc Lond, B, Biol Sci* 359, 1931–1944.

Ruan, Z., and Kannan, N. (2015). Mechanistic Insights into R776H Mediated Activation of Epidermal Growth Factor Receptor Kinase. *Biochemistry* 54, 4216–4225.

Runge, K.E., Evans, J.E., He, Z.-Y., Gupta, S., McDonald, K.L., Stahlberg, H., Primakoff, P., and Myles, D.G. (2007). Oocyte CD9 is enriched on the microvillar membrane and required for normal microvillar shape and distribution. *Dev Biol* 304, 317–325.

Schlessinger, J. (2002). Ligand-induced, receptor-mediated dimerization and activation of EGF receptor. *Cell* 110, 669–672.

Shan, Y., Eastwood, M.P., Zhang, X., Kim, E.T., Arkhipov, A., Dror, R.O., Jumper, J., Kuriyan, J., and Shaw, D.E. (2012). Oncogenic mutations counteract intrinsic disorder in the EGFR kinase and promote receptor dimerization. *Cell* 149, 860–870.

Shi, F., Telesco, S.E., Liu, Y., Radhakrishnan, R., and Lemmon, M.A. (2010). ErbB3/HER3 intracellular domain is competent to bind ATP and catalyze autophosphorylation. *Proc Natl Acad Sci U S A* 107, 7692–7697.

Slamon, D.J., Leyland-Jones, B., Shak, S., Fuchs, H., Paton, V., Bajamonde, A., Fleming, T., Eiermann, W., Wolter, J., Pegram, M., et al. (2001). Use of chemotherapy plus a monoclonal antibody against HER2 for metastatic breast cancer that overexpresses HER2. *N Engl J Med* 344, 783–792.

Sliwkowski, M.X., Schaefer, G., Akita, R.W., Lofgren, J.A., Fitzpatrick, V.D., Nuijens, A., Fendly, B.M., Cerione, R.A., Vandlen, R.L., and Carraway, K.L. (1994). Coexpression of erbB2 and erbB3 proteins reconstitutes a high affinity receptor for heregulin. *J Biol Chem* 269, 14661–14665.

Smith, A.W. (2015). Detection of rhodopsin dimerization in situ by PIE-FCCS, a time-resolved fluorescence spectroscopy. *Methods Mol Biol* 1271, 205–219.

Sonnleitner, A., Mannuzzu, L.M., Terakawa, S., and Isacoff, E.Y. (2002). Structural rearrangements in single ion channels detected optically in living cells. *Proc Natl Acad Sci U S*

A 99, 12759–12764.

Stamos, J., Sliwkowski, M.X., and Eigenbrot, C. (2002). Structure of the epidermal growth factor receptor kinase domain alone and in complex with a 4-anilinoquinazoline inhibitor. *J Biol Chem* 277, 46265–46272.

Ulbrich, M.H., and Isacoff, E.Y. (2007). Subunit counting in membrane-bound proteins. *Nat Methods* 4, 319–321.

Valley, C.C., Arndt-Jovin, D.J., Karedla, N., Steinkamp, M.P., Chizhik, A.I., Hlavacek, W.S., Wilson, B.S., Lidke, K.A., and Lidke, D.S. (2015). Enhanced dimerization drives ligand-independent activity of mutant epidermal growth factor receptor in lung cancer. *Mol Biol Cell* 26, 4087–4099.

Wassenaar, T.A., Ingólfsson, H.I., Böckmann, R.A., Tieleman, D.P., and Marrink, S.J. (2015). Computational Lipidomics with insane: A Versatile Tool for Generating Custom Membranes for Molecular Simulations. *J Chem Theory Comput* 11, 2144–2155.

Yang, T.T., Cheng, L., and Kain, S.R. (1996). Optimized codon usage and chromophore mutations provide enhanced sensitivity with the green fluorescent protein. *Nucleic Acids Res* 24, 4592–4593.

Yarden, Y., and Schlessinger, J. (1987a). Epidermal growth factor induces rapid, reversible aggregation of the purified epidermal growth factor receptor. *Biochemistry* 26, 1443–1451.

Yarden, Y., and Schlessinger, J. (1987b). Self-phosphorylation of epidermal growth factor receptor: evidence for a model of intermolecular allosteric activation. *Biochemistry* 26, 1434–1442.

Yarden, Y., and Sliwkowski, M.X. (2001). Untangling the ErbB signalling network. *Nat*

Rev Mol Cell Biol 2, 127–137.

Yildiz, A., Tomishige, M., Vale, R.D., and Selvin, P.R. (2004). Kinesin walks hand-over-hand. *Science* 303, 676–678.

Zhang, F., Wang, S., Yin, L., Yang, Y., Guan, Y., Wang, W., Xu, H., and Tao, N. (2015). Quantification of Epidermal Growth Factor Receptor Expression Level and Binding Kinetics on Cell Surfaces by Surface Plasmon Resonance Imaging. *Anal Chem* 87, 9960–9965.

Zhang, Q., Park, E., Kani, K., and Landgraf, R. (2012). Functional isolation of activated and unilaterally phosphorylated heterodimers of ERBB2 and ERBB3 as scaffolds in ligand-dependent signaling. *Proc Natl Acad Sci U S A* 109, 13237–13242.

Zhang, X., Gureasko, J., Shen, K., Cole, P.A., and Kuriyan, J. (2006). An allosteric mechanism for activation of the kinase domain of epidermal growth factor receptor. *Cell* 125, 1137–1149.

Zhen, Y., Caprioli, R.M., and Staros, J.V. (2003). Characterization of glycosylation sites of the epidermal growth factor receptor. *Biochemistry* 42, 5478–5492.